JET–P(97)03

Plasma Detachment in JET Mark I Divertor Experiments

A Loarte, R D Monk, J R Martín-Solís[1], D J Campbell, A V Chankin[2], S Clement, S J Davies, J K Ehrenberg, S K Erents[3], H Y Guo, P J Harbour, L D Horton, L C Ingesson, H J Jäckel, J Lingertat, C G Lowry, C F Maggi, G F Matthews, G K McCormick[4], D P O'Brien, R Reichle, G Saibene, R J Smith, M F Stamp, D Stork, G C Vlases.

JET Joint Undertaking, Abingdon, Oxfordshire, OX14 3EA, UK.
[1] Escuela Politécnica Superior, Universidad Carlos III de Madrid, Spain.
[2] and Scientific Centre Kurchatov, INF, Moscow, Russia.
[3] UKAEA Culham Laboratory, Abingdon, OX14 3DB, UK.
[4] Max Planck Institute for Plasma Physics, 85748 Garching, Germany.

Preprint of a paper to be submitted for publication in
Nuclear Fusion

February 1997

ABSTRACT

The experimental characteristics of divertor detachment in the JET tokamak with the Mark I pumped divertor are presented for Ohmic, L-mode and ELMy H-mode experiments with the main emphasis on discharges with deuterium fuelling only. The range over which divertor detachment is observed for the various regimes as well as the influence of divertor configuration, direction of the toroidal field, divertor target material and active pumping on detachment will be described. The observed detachment characteristics such as the existence of a considerable electron pressure drop along the field lines in the scrape-off layer, and the compatibility of the decrease in plasma flux to the divertor plate with the observed increase of neutral pressure and the D_α emission from the divertor region will be examined in the light of existing results from analytical and numerical models for plasma detachment. Finally, a method to evaluate the degree and window of detachment is proposed and all the observations of the JET Mark I divertor experiments summarised in the light of this new quantitative definition of divertor detachment.

1. INTRODUCTION

In recent years it has become evident that the problems of power deposition and wall erosion are of paramount interest to be addressed for the development of next-step tokamak devices such as ITER. While the high recycling divertor regime may be a marginally acceptable regime of operation from the viewpoint of power handling, the erosion associated with the large incident ion fluxes may limit seriously the lifetime of the divertor target, making the applicability of the high recycling divertor questionable for next step devices [1]. Furthermore, if the high recycling regime is extrapolated to some of the operating modes proposed for ITER even the power deposited onto the divertor by the recombining ions and electrons in the material surface will exceed the steady-state power handling capability of the divertor target [2]. As a solution to these two problems, the so-called “detached” divertor regime was first proposed to be the preferred divertor regime of a next-step device [3].

The basic physical features of the detached divertor rely upon the transfer of parallel momentum from the plasma to the recycling neutral atoms and subsequently to the divertor target and vessel walls. This has two important effects : the plasma pressure at the divertor is reduced with respect to that expected from the high recycling regime; and, together with ionisation losses and impurity radiation, it leads to low electron temperatures at the divertor which allow volume recombination processes to take place. The combination of the pressure reduction and hydrogen recombination leads to lower incident ion fluxes to the divertor target and potentially allows one to achieve higher radiative power fractions in the scrape-off layer (SOL) and divertor. This comes about because the recombination power deposited on the target decreases with the reduction of the plasma flux [4]. A further beneficial effect of the detached divertor regime is that the largest particle flux impinging on the surfaces is in the form of

hydrogenic neutral atoms and molecules scattered from the plasma, which are not accelerated by the sheath potential and hence have lower energies than the corresponding ions. This minimises the amount of physical sputtering suffered by the divertor target, although it is not expected to significantly reduce chemical sputtering from carbon based divertor targets.

A regime that displays most of the characteristics described above has been obtained in many divertor experiments by increasing the deuterium (or hydrogen) fuelling rate at constant input power [5, 6, 7, 8, 9, 10, 11, 12]. The basic features reported previously from JET experiments during the 1990/91 experimental campaign [5, 7] have been confirmed in the experiments carried out in JET with the Mark I Pumped Divertor but with a much improved diagnostic capability, which has allowed the quantitative characterisation of this regime.

The divertor configuration is obtained in the JET Mark I pumped divertor by using the four divertor coils at the bottom of the vacuum vessel. The divertor target is situated on top of these coils and consists of rows of tiles (made of Carbon (CFC) or Beryllium) with toroidal gaps that allow an efficient divertor pumping by means of the divertor cryopump. For further details of the JET Mark I divertor hardware and a summary of the experimental results the reader is referred to [13,14].

Dedicated experiments have been carried out during the JET Mark I pumped divertor 1994/95 experimental campaign to study the detached divertor regime. In this paper we report upon the detailed analysis of measurements obtained during these experiments and interpret them in the light of existing results from 1-D SOL analytical/numerical models and 2-D SOL computer codes for the plasma edge. In Section 2 we describe the experiments performed in JET together with the available diagnostic information. In Section 3 we concentrate on a detailed description of the evolution of the main plasma, SOL and divertor plasma parameters for few selected discharges in different confinement regimes as the fuelling is increased, causing the divertor to change from low to high recycling and ultimately access the detached regime. In Section 4 we describe the influence of additional factors on the detached divertor regime such as divertor geometry, wall clearance, divertor pumping and the effect on detachment of the toroidal field direction. In Section 5 we concentrate on the behaviour of impurities during divertor detachment, including the effect of different divertor target materials. In Section 6 we define and quantify the degree of detachment by extrapolation of experimental scaling laws for the high recycling regime and summarise the results of the JET Mark I detached divertor experiments in this new context. We use the new definition to illustrate concepts such as partial detachment and the window of tokamak operation in terms of main plasma density over which the detached divertor regime exists (detachment window). Finally, in Section 7 we summarise the findings of this paper.

2. DIAGNOSTICS AND EXPERIMENTAL METHOD

2.1 Diagnostic Systems

The range of diagnostics used to characterise the main plasma, SOL and divertor plasma has been very extensive in the JET Mark I Divertor 1994/95 experimental campaign. In addition to the routine diagnostics for the main plasma that provide measurements of density, electron and ion temperature, bulk plasma radiation and the concentration of impurities, the following diagnostics have been operated in the experiments described in this paper to characterise the plasma and hydrogenic neutrals in the main SOL and divertor region :

- Main plasma edge and SOL diagnostics :

  Reciprocating Langmuir Probe. Provides profiles of electron density and temperature in the main SOL.

  Main Chamber Visible Spectroscopy. Provides information on the influxes of deuterium and impurities that enter the plasma from the main chamber walls.

  Edge ECE Heterodyne Radiometer. Provides electron temperature profiles in the outer regions of the main plasma.

- Divertor diagnostics :

  Divertor Target Langmuir Probes. They provide detailed information on the ion flux, electron density and temperature profiles at the divertor target. With the use of 4Hz strike point sweeping, the radial resolution of these profiles approaches 2 mm at the divertor, limited only by the width of the probe tips.

  Divertor Microwave Diagnostics : They provide information on the line integrated and peak electron density across the inner or outer divertor leg.

  Divertor Infrared Thermography : Provides the power deposition profiles on the divertor target. Due to the large radiated power fraction during detachment, the power arriving at the divertor is usually very low and under the detection limit of the JET diagnostic. However, this diagnostic can be used with a different purpose for detached divertor experiments, in which very high electron densities ($n_e \approx 10^{20}$ - $10^{21} m^{-3}$) and low electron temperatures ($T_e \leq 5$ eV) are observed in the divertor region. The Bremsstrahlung emission of such a plasma in the wavelength of the JET IR diagnostic (1.6 mm) is sufficiently intense to be detected by this system and, hence, it can be used to estimate the maximum plasma density in the divertor region during detached divertor experiments.

Divertor Visible Spectroscopy : Provides the emission profiles of the recycling species in the divertor such as Deuterium, Carbon and Beryllium, which are used to estimate the influxes of these species into the divertor plasma.

Divertor Thermal Helium Beam : Provides electron temperature and density profiles along lines of sight at various heights above the divertor target.

Divertor VUV Spectroscopy : Provides the emission intensity of the spectroscopic lines that account for most of the radiation of the recycling species at the inner divertor.

Divertor Bolometers : They provide detailed information of the profiles of radiation in the divertor and are essential to follow the movement of the region of highest radiation intensity as detachment proceeds.

Divertor Pressure Gauges : These gauges are installed at various poloidal positions under the Mark I divertor target and provide information on the neutral flux to the divertor target and its poloidal distribution.

Figures 1.a-d show the spatial location of the various diagnostics described above together with one of the typical reconstructed MHD equilibria used for the experiments discussed in this paper.

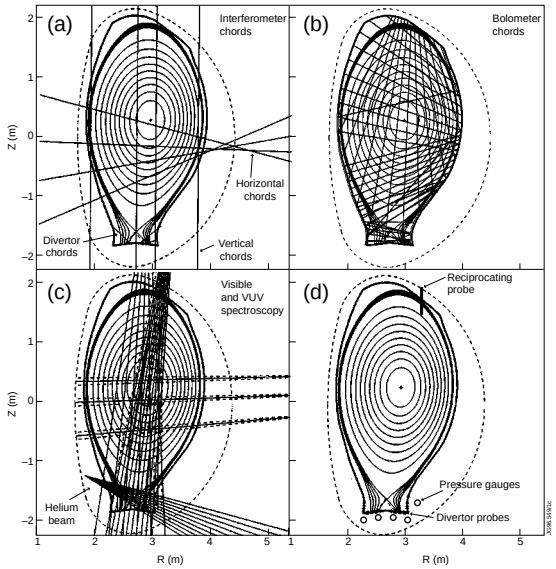

Fig.1: a) Lines of sight of the Divertor Microwave diagnostics and Main Chamber Interferometer. b) Lines of sight of the various Bolometer cameras in JET used to calculate the radiation emissivity profiles by tomographic reconstruction. d) Spatial location of the Divertor Langmuir Probes, Reciprocating Probe and Divertor Pressure Gauges. c) Lines of sight of various diagnostics used in this paper such as Visible Spectroscopy, VUV Divertor Spectroscopy and Thermal Helium Beam. A typical MHD equilibria used in the experiments described in the paper is shown for comparison.

2.2 Experimental Characterisation of Detachment in the Mark I Pumped Divertor

An exhaustive series of experiments has been performed to characterise divertor detachment in the JET Mark I pumped divertor including input power scans, divertor geometry scans, forward and reversed toroidal field comparison, variation of the divertor target material and the influence of active pumping. Only limited scans of the plasma current have been attempted given the high risk of disruptions for detached discharges operating in close proximity to the density limit. Consequently, most of the data presented in this paper corresponds to discharges with 2-2.5 MA of plasma current, which is a relatively low level of current for the JET device which is capable of operating divertor configurations at up to 6 MA [15].

The majority of the experiments performed to characterise detachment for Ohmic and L-mode regimes are discharges in which the main plasma density is increased slowly by deuterium gas fuelling, while maintaining constant levels of additional heating power (for L-mode discharges). The obvious advantage of this type of experiment is that different divertor regimes can be obtained under identical machine conditions. This removes the uncertainty introduced by insufficient characterisation of the machine conditions, which may vary within a given series of discharges. The disadvantage of this approach is the lack of true steady-state conditions for these experiments and one may call into question the relevance of such results. However, it has been found experimentally that, provided that the density ramps are performed slowly enough (with respect to the typical particle diffusion times), the density profiles have time to adapt to the changing particle balance. Under such conditions, the results obtained from these density ramps are similar to those obtained during steady-state density variation experiments in separate discharges, and hence the density ramps can be representative of a series of steady-state density points. Typical density ramp speeds that guarantee quasi steady-state particle balance in JET are 1.0-1.5 10^{19} $m^{-3}s^{-1}$ for Ohmic discharges and 1.5-2.0 $10^{19}m^{-3}s^{-1}$ for L-mode discharges. Acomparison of the measured maximum divertor ion fluxes versus line averaged density for a density ramp, together with the corresponding steady state discharges in L-mode is shown in Fig. 2 showing agreement to better than 15%.

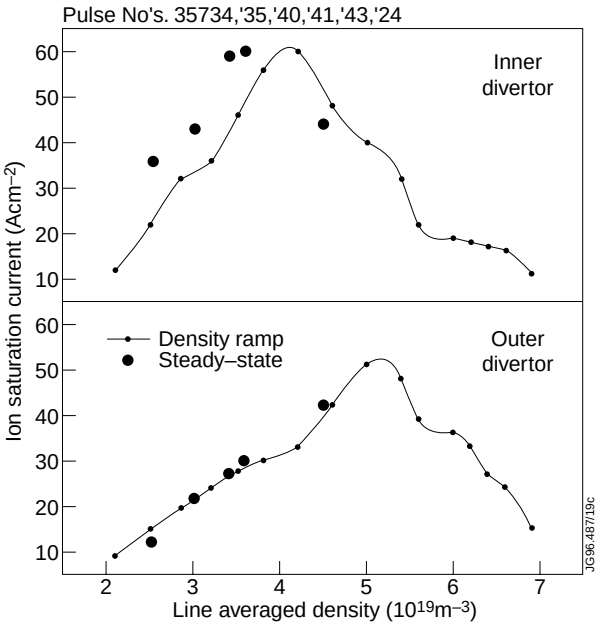

Fig.2: Measured peak ion fluxes at the inner and outer divertor for a density ramp in L-mode (4MW of NBI) compared to the corresponding discharges in steady state. The density at which detachment occurs at the inner divertor is found to differ by less than 15% in the two type of experiments.

In the case of ELMy H-mode discharges, density ramps are difficult to obtain experimentally since the density of the plasma appears to be more resilient to gas fuelling than in Ohmic and L-mode discharges. By using the divertor cryopump it has been possible to vary the main plasma density by up to a factor of two [16]. To study divertor detachment in this regime we have performed gas fuelling scans on a shot-by-shot basis, while the plasma density varies according to changes in the ELM behaviour caused by the level of gas fuelling.

3. BASIC OBSERVATIONS ON THE APPROACH TO DETACHMENT FOR DISCHARGES WITH FORWARD FIELD AND VARIOUS CONFINEMENT REGIMES

3.1. Ohmic Discharges

The typical evolution of the plasma parameters measured at the divertor and SOL during a quasi-steady state density ramp is shown in Fig. 3. With increasing main plasma density, the divertor evolves through a series of well defined phases which we describe in the detail in the following sections.

3.1.1. Low recycling divertor

This phase is characteristic of low plasma densities during which the measured temperature gradients along the field line are small. The losses of momentum in the SOL are small in this regime and, hence, the plasma pressure at the divertor target is a factor of two smaller than in the SOL, due to the acceleration of ions to the sound speed at the sheath. Numerical 2-D simulations of the SOL plasma show that most of the pressure drop from the SOL to the divertor target occurs in the ion channel [17]. Therefore, for this regime the electrons are in pressure balance over the whole of the SOL and divertor, within the experimental uncertainties of the position of the magnetic separatrix at the reciprocating Langmuir Probe and divertor target. These features have been commonly seen in most experiments [18, 19, 20]. In fact, we use the assumption of pressure balance during the low recycling phase to accurately determine the distance between the reciprocating probe and the magnetic separatrix. It is subsequently assumed that the absolute error between the estimate from magnetic measurements and that deduced by pressure balance during the low recycling phase remains constant throughout the discharge. Such a cross-calibration is needed to accurately determine the change in parallel electron pressure for detached regimes where electron pressure conservation is no longer applicable.

One consequence of the small parallel temperature gradients and pressure balance observed for low recycling divertors is that the divertor density is similar to that of the SOL since there is little amplification of the incident ion flux due to the re-ionisation of neutrals in the divertor. Under these conditions, it is found that the ratio of the total ion flux to the total D_α emission from the divertor is approximately 20, which is in good agreement with the calculated

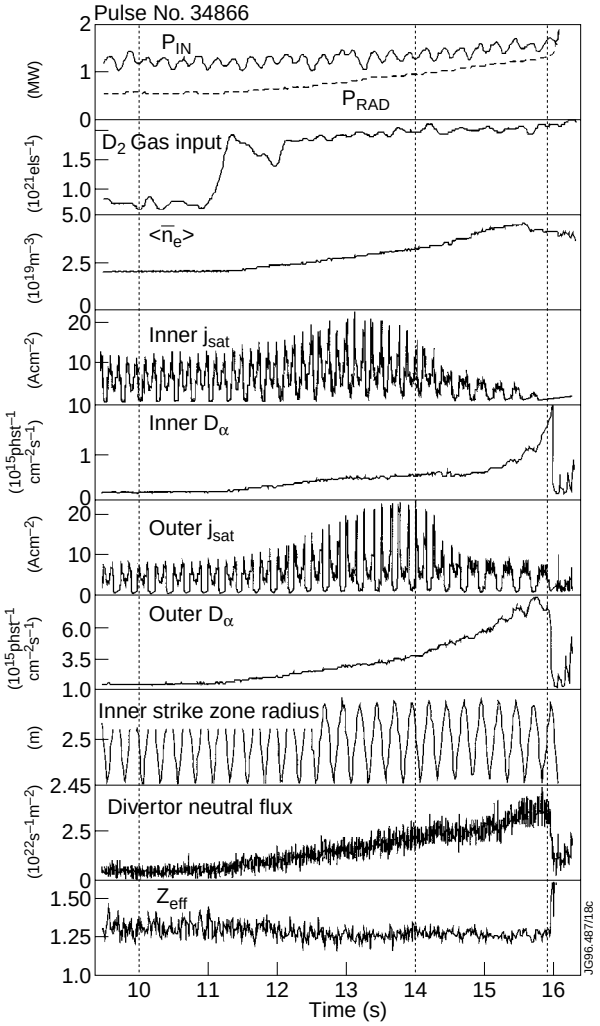

Fig.3: Evolution of the measured core and divertor plasma parameters during an Ohmic density ramp. (a) Ohmic power and radiated power, (b) D_2 gas fuelling rate, (c) Main plasma line average density, (d) Inner divertor ion flux, (e) Average inner divertor D_α photon flux (note the increase of D_α as the ion flux decreases characteristic of divertor detachment), (f) Outer divertor ion flux, (g) Average outer divertor D_α photon flux, (h) Radius of the inner strike point on the divertor target (4 Hz strike point sweeping), (i) Neutral hydrogen flux in the subdivertor module at the cryopump location, (j) Main plasma Z_{eff} (note that it does not increase as the main plasma density increases). The vertical dashed lines indicate the times at which the upstream SOL profiles measurements are taken with the reciprocating probe.

Johnson-Hinnov factor [21] (ionisations per D_α photon emitted) for these measured plasma conditions. The profiles of electron pressure, density and temperature at both divertors and in the SOL are shown in Fig. 4. It is important to note that while the electron pressure is similar at both divertors, the inner divertor electron temperature is much lower than that of the outer one and, hence, its density is much higher. This observation is typical of discharges with forward toroidal field [22, 23] and causes the inner divertor to access the high recycling and detached divertor regimes at lower main plasma densities. Hence, in this figure only the outer divertor is in the low recycling regime while the inner divertor has already accessed the high recycling regime which is described below.

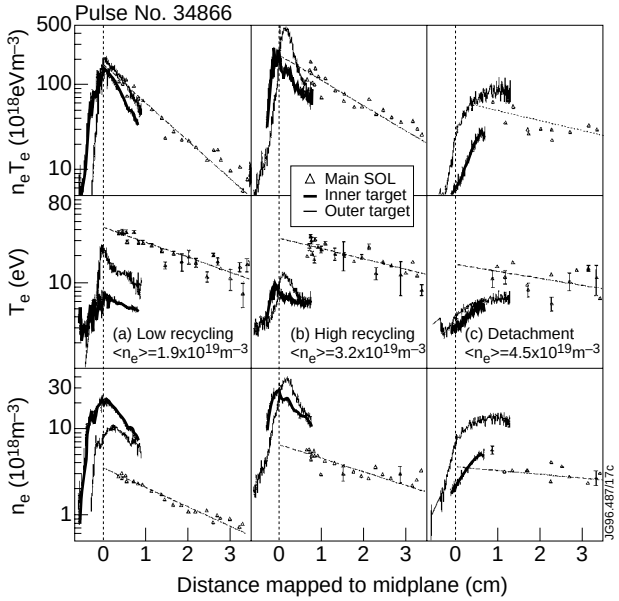

Fig.4: Electron pressure, temperature and density in the SOL (triangles) and the divertor (thick line inner divertor, thin line outer divertor) versus distance to the separatrix mapped to the outer midplane at three different times during an Ohmic density ramp discharge: low recycling, high recycling and detached divertor.

3.1.2. High recycling divertor

As the main plasma density increases, the divertor enters the high recycling regime in which large electron temperature gradients along the field line are measured and large amplification of the plasma flux is observed at the divertor target. However, parallel electron pressure balance remains approximately conserved along the whole SOL and divertor and consequently the divertor density is considerably higher than the SOL density. For the discharge shown in Fig. 3 and Fig. 4 the peak outer divertor density increases approximately with $\langle n_e \rangle^4$ during this phase, while the temperature decreases as $\langle n_e \rangle^{-2}$. This results in a approximate increase of the measured peak ion flux with $\langle n_e \rangle^3$. These trends hold with increasing density until the separatrix divertor temperature reaches a value of 3 - 5 eV, at which point the peak ion flux density ceases to increase with main plasma density (more quantitative comparisons for various discharges and conditions will be described in Section 6). During the high recycling phase it is frequently observed the appearance of very peaked ion flux profiles which we will describe at the end of this section. Associated with this observation is the existence of a region close to the separatrix in which the electron pressure at the target exceeds the SOL electron pressure, as show in Fig. 4 for the outer divertor. While the detailed mechanism that leads to this over-pressure remains unclear, this phenomena is commonly observed in other divertor experiments such as in high recycling discharges in Alcator C-Mod [24] where it is known as “death rays”.

The achievement of low temperatures at the divertor is observed to be fundamental to trigger the so-called “roll-over” and divertor detachment phase in all divertor experiments [8, 20, 25, 26]. As the ion flux increases with main plasma density, the neutral hydrogen pressure

under the divertor and the D_α emission from the outer divertor also increase (see Fig. 3). The ratio between the integrated ion flux to the integrated D_α emission from the outer divertor drops from the value of 20, typical of low recycling conditions, to values of 5, which is consistent with the corresponding decrease in temperature and increase in density observed at the outer divertor.

During the high recycling phase, the upstream SOL density profiles broaden considerably (see Fig. 4), as expected from the enhanced ionisation in the divertor and the smaller neutral hydrogenic leakage to the main plasma. However, the divertor density profiles show a clear steepening in the region near the separatrix, which reflects the fact that local ionisation, radiation and transport processes are dominating the divertor plasma during this phase [27]. The inner divertor undergoes the same transitions seen at the outer divertor but at lower main plasma densities and, hence, while the outer divertor is in the high recycling regime, the inner divertor has started to detach.

It is important to note that the main SOL separatrix electron pressure increases from the low recycling to the high recycling phase, which is consistent with the increase in main plasma density and the fact that the power that crosses the separatrix, as estimated from the input power and the bolometers, stays approximately constant during this evolution. During the high recycling phase, the radiation emission peaks near the divertor target and is very localised within the divertor legs, as deduced from tomographic reconstructions of measurements by bolometer cameras in the divertor. In the next section we present detailed measurements of the divertor radiation profiles and the way in which they evolve as detachment progresses.

3.1.3. Roll-over and Detachment phase

The beginning of the roll over phase is marked by the start of a plateau in the time evolution of the peak ion flux to the divertor target as the density increases. This is the primary experimental indication that detachment processes are occurring in the divertor. The typical level of radiated power at the so-called “roll-over” phase is around 55-70% of the total input power depending somewhat on the machine conditions and magnetic configuration. The roll-over phase starts first at the inner divertor and the subsequent time evolution is similar for both divertors, although the level of detachment reached at the inner divertor is larger than that of the outer one when the density limit is attained. Initially, only the ion flux near the separatrix ceases to increase with density, while it still rises in the outer regions of the SOL. As the density increases further, the ion flux near the separatrix starts to fall, while the flux to the outer regions in the SOL may be still increasing. This fall of the ion flux marks the beginning of the detachment phase. The region over which the ion flux drops widens with increasing density (detachment region) until the radiation escapes the divertor region and a MARFE [5] is formed in the main plasma and the discharge eventually disrupts. Fig. 5 shows the evolution of the ion flux to the inner and outer divertors at various distances from the separatrix (mapped to the outer midplane). It is clear from this figure that the degree of detachment (measured by the ion flux drop) and the extent of

the detachment region is considerably larger at the inner than at the outer divertor. From this figure it is also observed that, close to the main plasma MARFE formation, the ion flux has dropped everywhere at the inner divertor while is still increasing in the outer regions of the SOL at the outer divertor. This is the typical observation in JET and is characteristic of so-called partial detachment, in which the ion flux close to the separatrix is reduced while there is a significant flux in the outer SOL. This may be contrasted with the total detachment typically observed at the inner divertor during which the ion flux drops everywhere across the whole profile.

The detailed divertor ion flux measurements obtained in the JET Mark I divertor have eliminated the hypothesis that enhanced anomalous perpendicular transport in the divertor explains plasma detachment, as

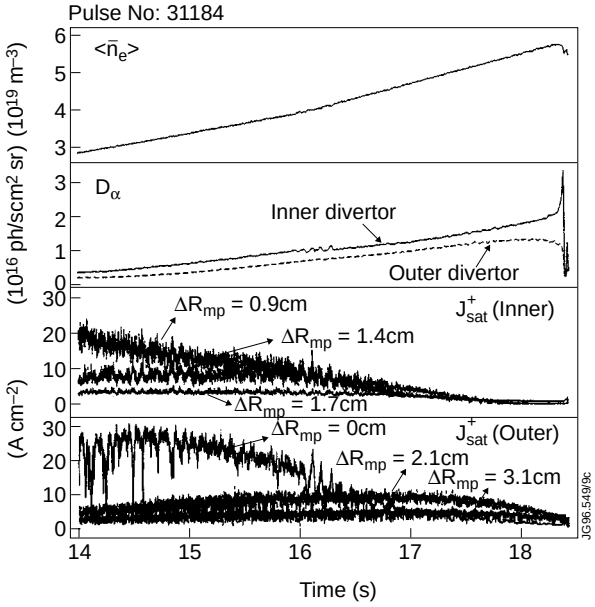

Fig.5: Evolution of the ion flux at several distances from the separatrix for an Ohmic density ramp in JET. Note that while the ion flux drops with increasing density close to the separatrix at the outer divertor, it increases continuously away from it (partial detachment). At the inner divertor the ion flux drops at all radial positions as the density increases (total detachment).

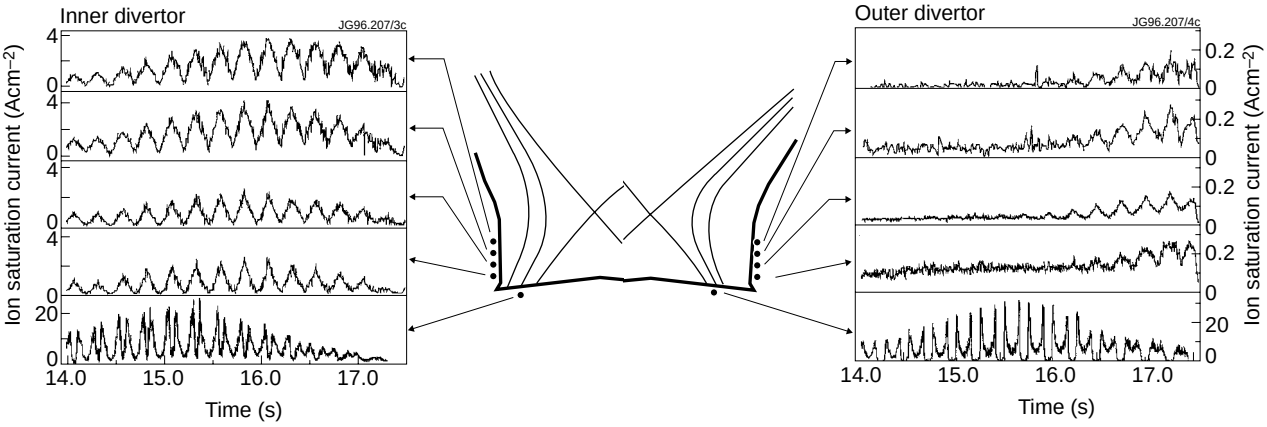

Fig.6: Evolution of the ion flux at the inner and outer horizontal divertor and the inner and outer vertical plates for an Ohmic density ramp in JET. The modulation of the ion flux measurements is due to strike point sweeping during the discharge. There is no indication of a strong increase of the ion flux on the vertical plates beyond the roll-over phase, as the ion flux to the horizontal plate decreases.

observed in linear devices [28]. According to this mechanism, the low electron temperature and high neutral densities, characteristic of detached divertors, produce an enhanced perpendicular transport which increases radial particle losses to the side walls, thereby reducing the parallel ion flux incident on the horizontal divertor target. This process is not observed experimentally as shown in Fig. 6, where the time evolution of the ion flux to probes in the horizontal inner and

outer divertor targets and embedded in the side walls (which can be used as vertical divertor target) of the JET Mark I divertor are shown. These observations demonstrate that the ion flux drop to the horizontal divertor does not lead to any significant increase of the ion flux to the side walls, besides that associated with the increase of the main SOL plasma density in the outer regions of the SOL which follow the main plasma density increase (note that the measured values of the ion flux to the side walls are one to two orders of magnitude lower than those measured at the horizontal target).

The beginning of the roll-over and detachment phase is correlated with the electron temperature in the divertor achieving values around 5 eV, as expected from simple models of plasma detachment [29, 30]. Fig. 7 shows the evolution of the separatrix electron pressure, density and temperature (measured with Langmuir probes and CII VUV line ratio techniques) for the inner and outer divertor during such a density ramp. As the main plasma density increases the divertor temperature decreases and, correspondingly, the divertor density increases maintaining a constant or increasing divertor pressure. When the electron temperature reaches values close to 5 eV the electron pressure starts to decrease (as does the peak ion flux to the divertor) indicating the onset of detachment.

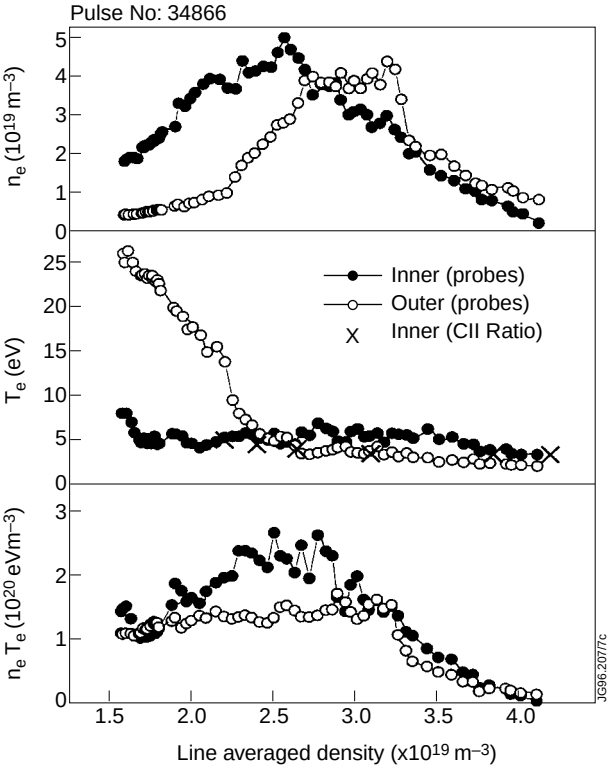

Fig.7: Evolution of the separatrix electron density, temperature and electron pressure measured with Langmuir probes at the inner and outer divertor for an Ohmic density ramp in JET. Measurements of the electron temperature deduced from CII VUV line ratios (904Å and 1335Å) for the inner divertor at several densities during the discharge are shown for comparison.

It is important to remark that during the high recycling and roll-over phase the Langmuir I-V characteristics measured by the divertor probes deviate from the idealised exponential form, which is usually utilised for the interpretation of these measurements. In particular, low ratios of electron to ion saturation currents are usually measured and typical resistive behaviour of the electron current is seen at the inner divertor [31]. To correct for the low electron saturation currents, we analyse the measurements following the "virtual" double probe approach of Günther [32]. However, while the resistive effects are qualitatively described by the resistive probe model of Günther [33], this model is, in its present formulation (slab geometry among other assumptions), too simple and its application to the experiment does not produce satisfactory results. Hence, we have not applied any correction for the resistive effects seen at the inner divertor which may lead

to an overestimate of the real electron temperature. This fact is routinely confirmed by measurements of the inner divertor electron temperature with line ratios of CII (904Å and 1335Å) for the same discharge, which are also shown in Fig. 7. It is important to note that these spectroscopic measurements are not localised at the divertor plate but intrinsically linked to the ion emitting the line (C^+) and, hence, are affected by the change in the ionisation mean free path of neutral carbon. This is particularly important for the detached phase, during which the temperature determined by this method is likely to reflect the electron temperature near the X-point, where most of the radiation is emitted, as will be described later. Hence, under these conditions, the actual electron temperature at the plate is likely to be lower than that determined using line ratio methods.

During the final stages of detachment, the separatrix electron temperature at the outer divertor (determined from Langmuir probes) drops to values in the region of 2-3 eV. This drop of electron temperature has also been confirmed by measurements from a thermal Helium beam diagnostic [34], which views across the outer divertor leg at various heights from the target up to the X-point region. Fig. 8 shows such observations for an Ohmic density ramp : with increasing density the electron temperature in the whole divertor leg decreases. Finally, when detachment is achieved the region of low temperature ($T_e \leq 10$ eV) expands along the field lines from the divertor target up to the X-point. The final stage of the detachment process is achieved when total detachment is reached at inner divertor and, subsequently, the region of high radiation moves away from the divertor and a MARFE develops in the main chamber.

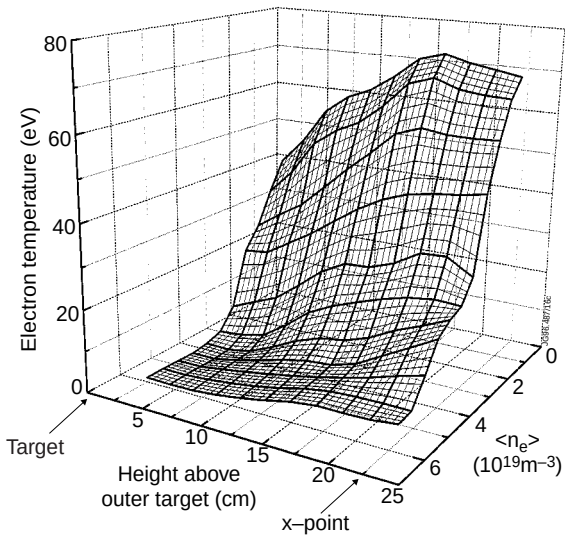

Fig.8: Profiles of electron temperature at the outer divertor leg from thermal Helium beam measurements for an Ohmic density ramp, as a function of the height above the divertor target and main plasma line average density. At the highest densities the outer divertor is partially detached and a region of low electron temperature extends between the divertor target and the X-point.

We will now consider in more detail the experimental observations that characterise divertor detachment, specifically, the increase of the divertor D_α and neutral pressure in the subdivertor volume as the main plasma density increases, despite the drop in the ion flux to the divertor plates. In principle, this seemingly contradictory observation can be qualitatively reconciled with the model for divertor detachment proposed by Stangeby [29], in which the plasma momentum flux is reduced by charge exchange collisions with recycling neutrals in the divertor. As the divertor electron temperature decreases to values approaching 5 eV, the charge-exchange

processes in the divertor begin to dominate over ionisation, and neutrals produced at the divertor plate have a very large probability of being scattered back to the divertor before they are ionised. In this process the neutrals can carry to the target a significant fraction of the momentum of the incoming ions and, therefore, decrease the ion flow to the divertor. This mechanism removes the apparent incompatibility of a low ion flux and a high neutral pressure in the subdivertor module. The decrease of the Johnson-Hinnov factor with decreasing temperatures also removes, in principle, the apparent incompatibly of a decrease in the divertor ionisation source (decrease in the ion flux to the divertor) and the large D_α emission. As the temperature decreases, the number of ionisations per D_α photon decreases and, correspondingly, the D_α emission increases for a given ionisation source.

However, when a detailed quantitative analysis of the measurements is performed, some difficulties for this relatively simple picture arise. Firstly, the behaviour of the peak ion flux and its integral is substantially different for both divertor targets. This is illustrated in Fig. 9 for an Ohmic density ramp : the peak ion flux decreases by a factor of 5 for the outer divertor during the detachment process while the integral barely decreases from its highest value (high recycling point) during the roll-over and detachment phase (characteristic of partial detachment). In the case of the inner divertor the picture is completely different, as both the peak ion flux and integral, decrease by more than an order of magnitude during the roll-over and detachment phase (characteristic of total detachment). Using the measured total ion flux to both divertors, we have derived an empirical Johnson-Hinnov factor and compared it with that derived from the measured divertor parameters and using the atomic data from the ADAS [35] database (Fig. 10). While it is clear that the change in the Johnson-Hinnov factor is similar to that expected for the variation of plasma parameters (and the small total ion flux drop) at the outer divertor during detachment, there is a large discrepancy between the calculated and measured factor for the inner divertor. Experimental uncertainties in the exact value of the electron temperature at the inner divertor do not allow a more precise determination of this discrepancy but are not enough, on their own, to explain this discrepancy For example, assuming T_e = 2eV and $n_e=10^{18}m^{-3}$ for detached divertor conditions results in ~1 photon per ionisation compared

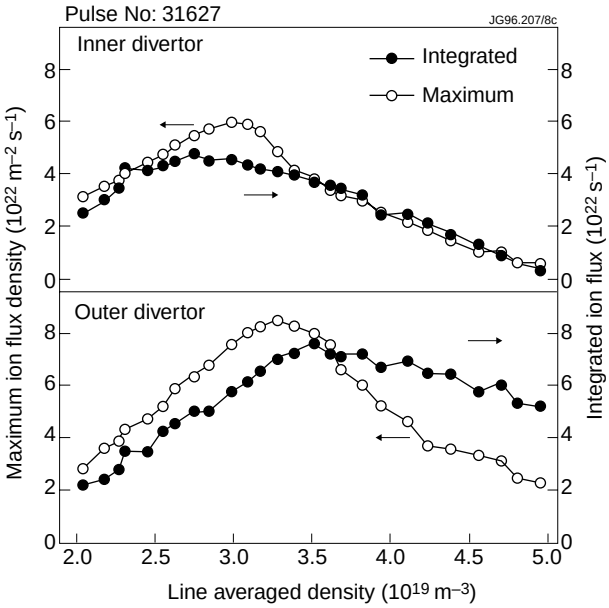

Fig.9: Outer and inner divertor peak and integral ion fluxes for an Ohmic density ramp. The outer divertor shows a decrease of the peak ion flux with density, while the integral ion flux remains approximately constant, which characterises partial divertor detachment. The inner divertor shows a large decrease of the peak ion flux and its integral, which is characteristic of total divertor detachment.

with <0.1 for the directly measured value at the inner divertor.

This discrepancy for the inner divertor is typical of totally detached divertors (only seen at the inner divertor in JET). It provides an indication that additional processes which modify the ionisation balance, such as recombination, and the distribution of the deuterium atoms in the different excited states (such as L_α re-absorption [36]), are taking place in the experiment, during total divertor detachment. There is indeed experimental evidence of these phenomena, for instance, in the increase of the measured ratio D_γ/D_α from the divertor as detachment proceeds. This observation indicates that the excited levels of the deuterium atoms are more populated than the normal distribution governed by electronic excitation/de-excitation consistent with deuterium recombination taking place (see Fig. 11). For some detached divertor discharges, it is also observed that there is a decrease of the ratio L_β/D_α [37] which indicates that radiation re-absorption is also taking place at the inner divertor (L_α would be strongly reabsorbed for such conditions). The detailed interpretation of these measurements needs highly sophisticated atomic population calculations [38], in conjunction with realistic plasma modelling [39] for these conditions. It is important to assess with these models the role and mechanisms of the plasma recombination processes that occur during total divertor detachment [17], as proposed in [40] on the basis of simulation studies of the maximum drop of the ion flux associated with momentum removal by neutral particle interaction in the divertor.

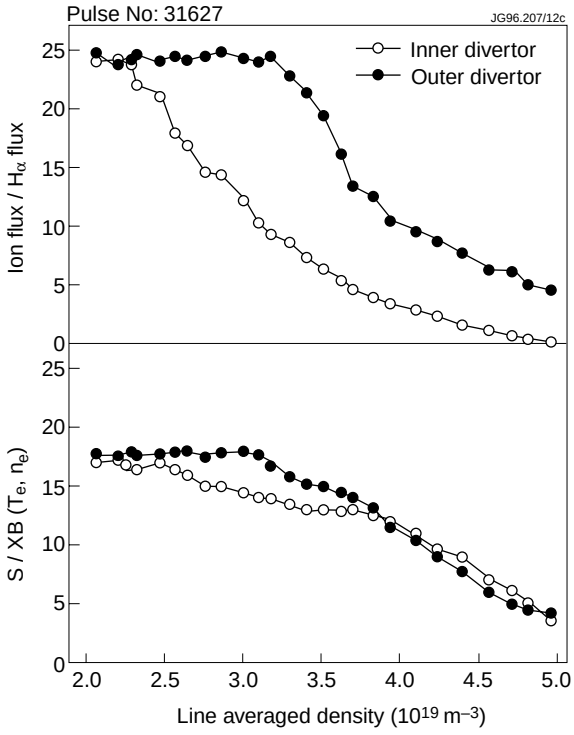

Fig.10: Experimentally determined (Top) and calculated (Bottom) Johnson-Hinnov factors for the inner and outer divertors for an Ohmic density ramp in JET. The experimental Johnson-Hinnov factor for the inner divertor changes by approximately two orders of magnitude from the low recycling to the detached phase.

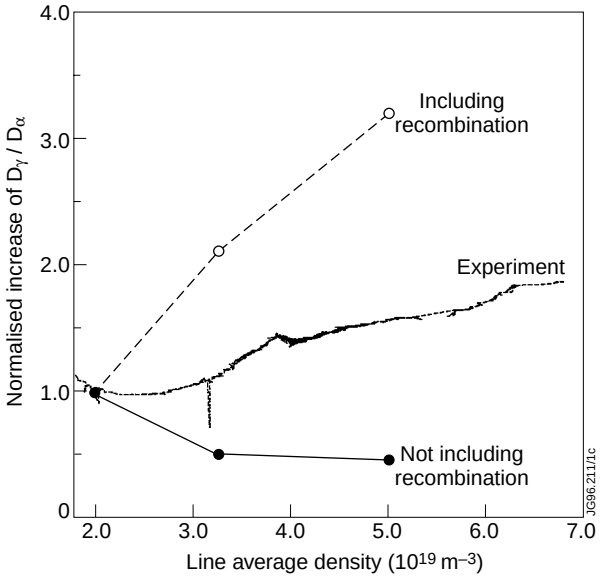

Fig.11: Evolution of the D_γ/D_α ratio with increasing density for an Ohmic density ramp in JET. Also shown are simulations with the EDGE2D/U-NIMBUS code of these conditions and the effect of including or excluding recombination in the computation of these line ratios [17].

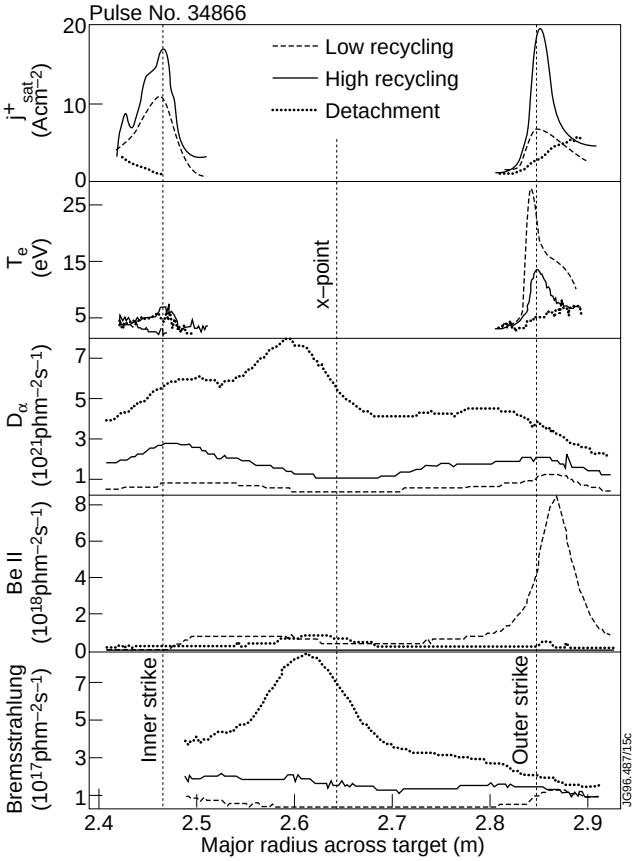

Fig.12: Profiles of ion flux, electron temperature, D_α, BeII and visible Bremmstrahlung emission from the divertor during low recycling, high recycling and divertor detachment, for an Ohmic density ramp in JET.

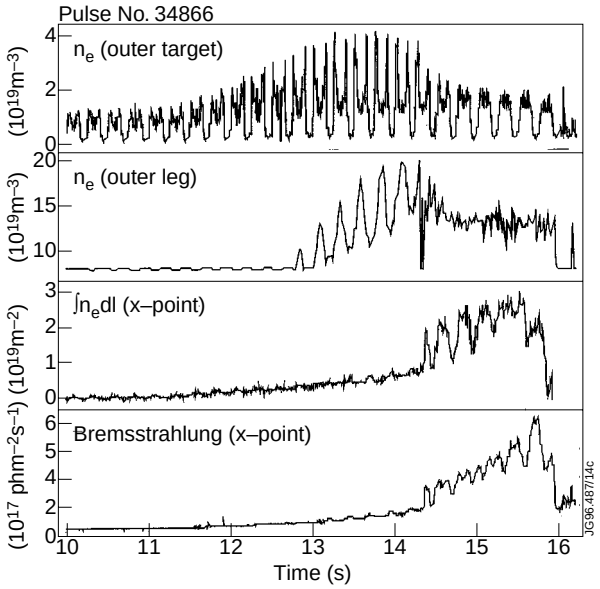

Fig.13: Evolution of the plasma density for an Ohmic density ramp in JET at various locations within the divertor : target, divertor leg and X-point. These are measured respectively by the Langmuir Probes embedded in the target, a microwave diagnostic that views across the divertor leg between the target and the X-point and an interferometer channel that passes through the X-point. The visible Bremsstrahlung emission at the X-point is also shown for comparison.

At the final stages of divertor detachment, the D_α emission and the radiation migrates towards the X-point, where a very dense radiating region is formed (with MARFE-like structure). An example of such divertor D_α emission behaviour is shown in Fig. 12, together with the visible Bremmstrahlung emission measured at the same position. From the Bremsstrahlung emission, it is clear that a very dense and cold plasma region is formed in the vicinity of the X-point, with densities of the order of 10^{20} m^{-3} [10]. These are indeed the densities which are measured at the divertor leg and the X-point with the microwave and interferometer diagnostics for these discharges, as shown in Fig. 13. The region of highest density moves away from the divertor (outer target), up the divertor leg (outer leg), towards the X-point (X-point), where the Bremsstrahlung emission increases considerably, until the radiation escapes from the divertor and a main plasma MARFE is formed. The same picture of migration away from the target towards the X-point can be drawn from the line integral of the bolometers located at the divertor,

which is shown in Fig. 14. It is important to note that at the very late stages of detachment, the peak of the radiation emission is located well above the X-point in the main plasma. This is in agreement with the measurements of the reciprocating probe shown in Fig. 4, that display a substantial pressure drop at the main SOL separatrix, consistent with the decreased power flux across the separatrix. Despite the migration of radiation above the X-point region, the impurity concentration in the main plasma, as measured by Z_{eff} derived from visible Bremsstrahlung, does not change significantly (as shown in Fig. 3). This indicates that either the impurity concentration in the main plasma is not dominated by the divertor or that the impurities are well confined in this MARFE-like structure and do not diffuse into the main plasma, despite their proximity to it during the detached divertor phase.

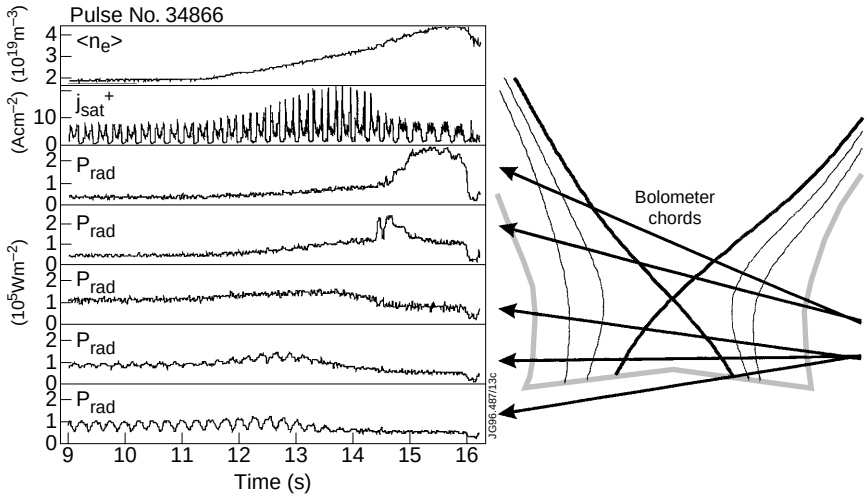

Fig.14: Evolution of the measured radiation along various chords within the divertor showing the migration of the radiation towards the X-point during the detachment process.

The use of strike point sweeping during these density ramp experiments has allowed the detailed characterisation of the shape of the ion flux profiles from the low recycling to the detached regime. It is routinely observed that during the transition from the low recycling to the high recycling regime ion flux profiles at the divertor develop a double peaked structure with the dominant peak growing from the private flux region side of the separatrix [27]. This peak finally dominates the ion flux profiles during the high recycling phase and disappears as detachment proceeds. There are indications that the formation of these peaks is related to anomalous transport in the SOL and divertor region but the detailed structure of these high recycling peaks has not been yet successfully reproduced [17]. Fig. 15 shows the measured ion flux profiles at the outer divertor target during an Ohmic density ramp to detachment where the evolution of the high recycling peaks is clearly displayed. Similar observations of peaked ion profiles during high recycling conditions have been made in Alcator C-Mod [24] where they are known as “death rays”. In this experiment the appearance of these peaks has been linked to anomalous transport of perpendicular momentum [17] in vertical plate divertors. Although this mechanism

describes satisfactorily the observations of vertical plate discharges in Alcator C-Mod, it cannot explain the observations from JET Mark I horizontal plate discharges.

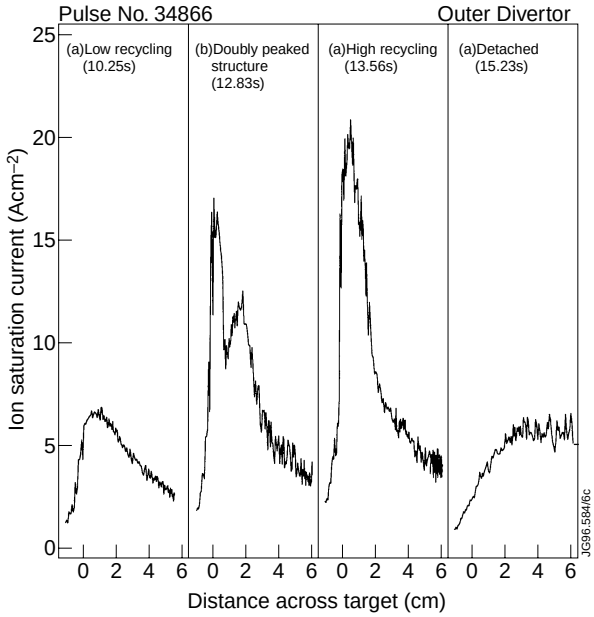

Fig.15: Measured ion flux profiles at the outer divertor during an ohmic density ramp discharge. With increasing density the profiles develop a second peak which grows from the private flux region side of the separatrix and dominates the ion flux profiles during the high recycling phase (13.56 s). This peak disapears during the partially detached phase (15.23 s).

3.2. L-mode Discharges

Similar general trends to those described above for Ohmic discharges are also observed in L-mode neutral beam heated discharges. Hence, our description of the processes taking place in L-mode discharges will be less detailed than that for the Ohmic discharges. A comparison of general observations in Ohmic and L-mode detachment is shown in Fig. 16, for two consecutive discharges of which one is Ohmic and the other has 2 MW of additional heating. The L-mode discharge exhibits the characteristics of detachment at a higher density than the Ohmic one and also reaches higher densities before the MARFE is formed in the main plasma, as expected from simple arguments based on the temperature of the divertor reaching a given low value ($T_e \leq 5$ eV)

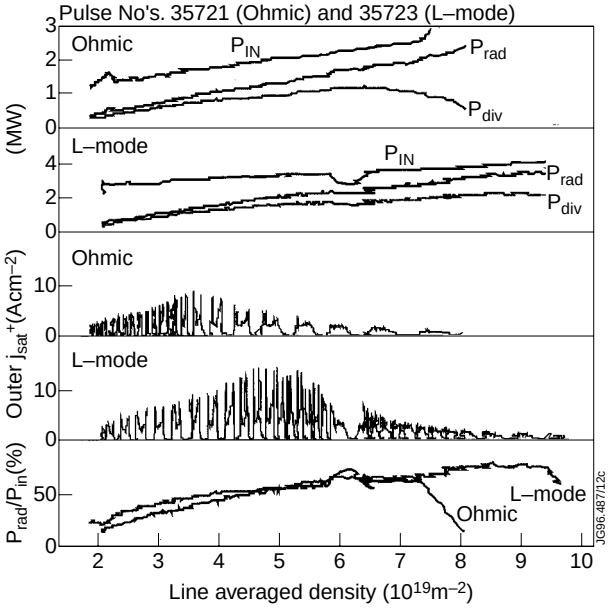

Fig.16: Evolution of the input power, measured radiation (total, bulk and divertor), ion flux to the outer divertor and percentage of total radiated power versus main plasma density for two similar discharges in Ohmic and L-mode with 2MW of additional heating.

when detachment sets in. This trend of increasing density with increasing power weakens at higher additional heating power as the divertor radiative losses increase to compensate.

As a consequence of the increase in divertor radiative losses, the overall increase in density range for L-mode discharges obtained by using additional heating is much smaller than that deduced from simple scalings based on power balance arguments such as $n_s \propto P_{input}^{5/8}$ [41], where n_s is the separatrix density (which is assumed to be proportional to the average density) and P_{input} is the total input power. This subject will be discussed in more detail in section 6, where the concept of the detachment window is introduced. The total radiation level at which detachment starts for Ohmic and L-mode discharges is typically around 50-60 % (composed of 30-40% divertor and X-point radiation and 10-20% bulk radiation), for which around 50% of the power that enters the SOL is radiated in the divertor.

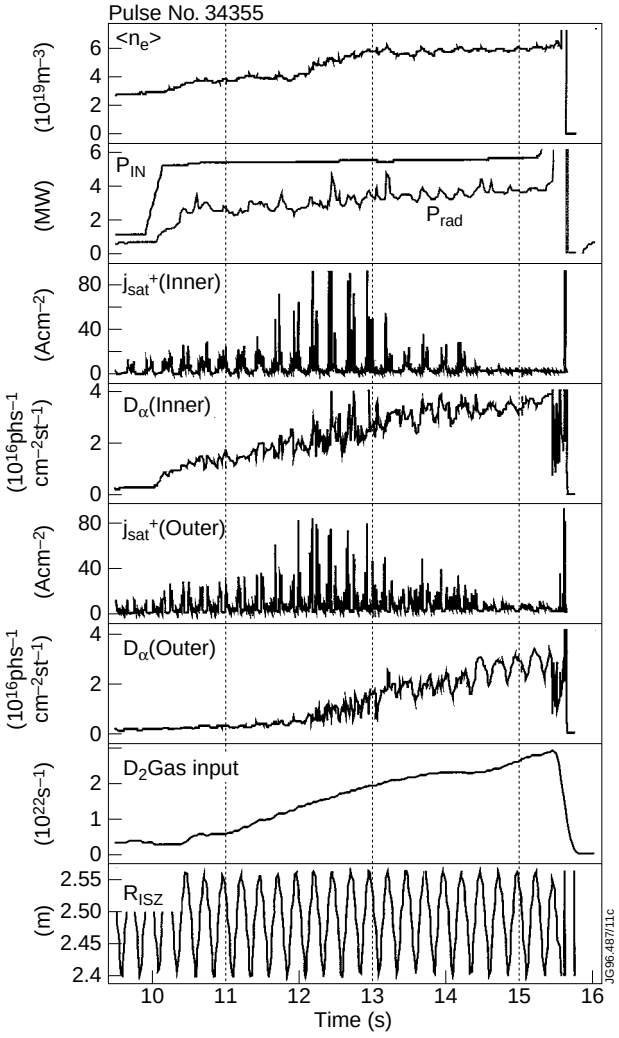

Fig.17: Evolution of main plasma and divertor parameters for an L-mode density ramp in JET (4.6 MW of additional heating). The vertical dashed lines indicate the times at which the upstream SOL profiles measurements are taken with the reciprocating probe.

Measurements taken during an L-mode density ramp to detachment (Fig. 17) confirm the experimental observations in Ohmic discharges, with the appearance of a pressure drop along the field line, when the divertor electron temperature reaches values close to 5 eV, as measured by Langmuir probes. The main SOL profiles (Fig. 18) broaden as the main plasma density increases and, for instance, the pressure profile e-folding length mapped to the outer midplane increases from 1.3 cm to 1.6 cm at the beginning of detachment and finally to 2.1 cm just before the MARFE escapes the divertor. The broadening of the density profile is the dominant term in this pressure profile broadening (2.2 cm (low recycling), 3.3 cm (high recycling), 4.0 cm (detached)) which raises questions about the possibility of having low interaction with the walls (high wall clearance) under high recycling and detached divertor conditions. This observation also calls into question the influence of the detailed design of the divertor under such detached conditions. In contrast to the Ohmic discharge shown above (Fig. 4), for L-mode discharges the pressure in the main SOL, measured by the reciprocating probe, does not decrease even at

the very late stages of detachment. This is consistent with a significant proportion of the input power still crossing the separatrix during this phase.

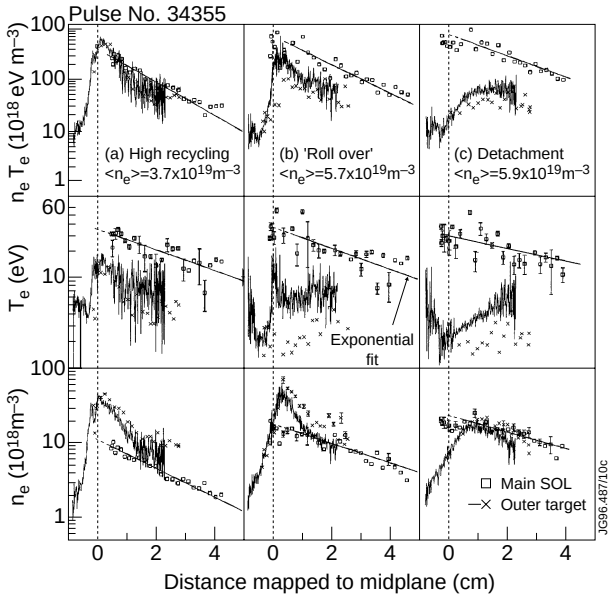

Fig.18: Main SOL and outer divertor profiles of electron pressure versus distance from the separatrix at the outer midplane, at three stages for the same L-mode density ramp shown in Fig. 17. Note the pressure drop of more than an order of magnitude during the detached phase of the discharge. During this phase the electron temperature is 2 - 3 eV at the outer divertor target, as measured with Langmuir Probes.

Using the measured D_α emission from the divertor and the integrated divertor ion flux we have calculated the empirical Johnson-Hinnov factor for the L-mode density ramp shown in Fig. 17. It exhibits the same trend observed for Ohmic discharges which indicates that recombination is taking place, when total detachment is obtained in the inner divertor (Fig. 19). The parameter that controls the on-set of plasma detachment is also the electron temperature as seen in Ohmic discharges, which reaches low values (under 5 eV) when detachment sets in. These low values are also confirmed by spectroscopic observations (CII VUV line ratios for the inner divertor and thermal Helium beam for the outer divertor), as it is shown in Fig. 20 for an L-mode density ramp.

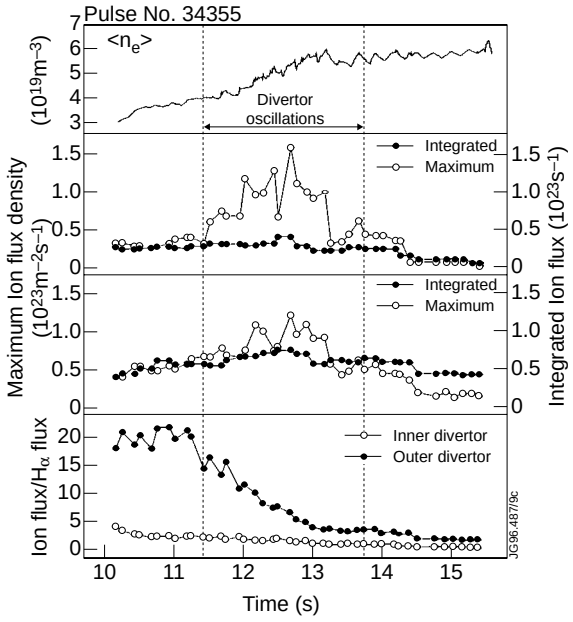

Fig.19: Peak and integrated ion fluxes to the inner and outer divertors for the same L-mode density ramp shown in Fig. 17. The inner divertor shows the typical drop of the peak and integral ion flux, characteristic of total divertor detachment, while the outer divertor shows the drop of the peak value but not its integral, characteristic of partial divertor detachment. The empirical Johnson-Hinnov factors derived from the integral ion flux and the measured divertor D_α emission are also shown for comparison.

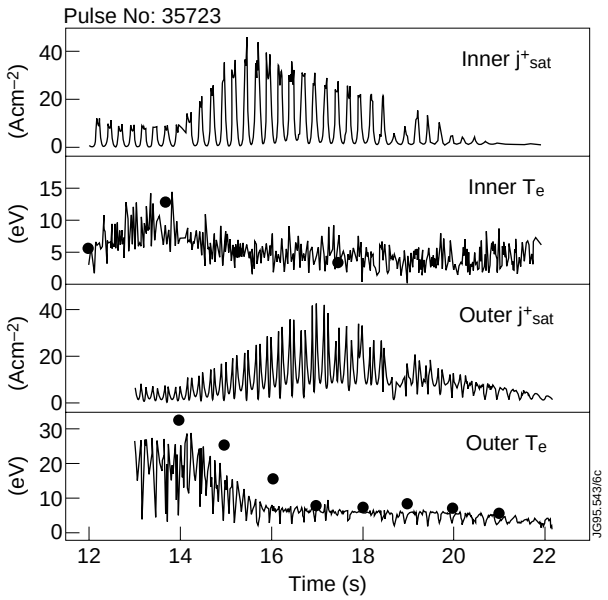

Fig.20: Evolution of inner and outer divertor ion flux and electron temperature for an L-mode density ramp. The values of the electron temperature measured with Langmuir probes are in reasonable agreement with spectroscopic measurements from line ratios (CII VUV line ratios for the inner divertor and thermal Helium beam for the outer divertor).

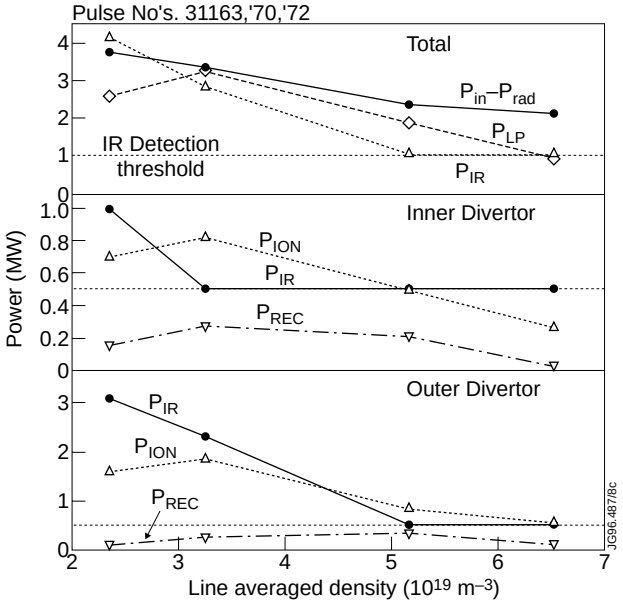

Fig.21: Power deposited onto the divertor from main plasma (radiation and input power) and IR thermography (P_{IR}) and derived from Langmuir probes ($P_{LP} = P_{ION} + P_{REC}$) for a series of L-mode discharges with increasing densities to divertor detachment. The top figure shows the total power balance, the central figure shows the power balance for the inner divertor (P_{ION} is the sheath power measured with Langmuir probes and P_{REC} is the recombination power) and the bottom figure the outer divertor. The power that is deposited on to the divertor target as the plasma flux recombines (P_{REC}) is shown for comparison and is observed to decrease during plasma detachment.

One of the main characteristics that makes detached divertor regimes attractive for next-step devices is related to the increase of the radiated power and plasma density in the divertor region, since not only is the erosion of the components reduced by the reduction of the ion flux, but also volumetric losses (including ion-neutral interactions) in the divertor dominate and the power deposited at the divertor target decreases. This is indeed observed in the experiment, as shown in Fig. 21 for an L-mode density scan. In this figure we compare the power deposited onto the inner and outer divertor plates as measured by the Langmuir probes (P_{LP}) and IR thermography (P_{IR}). As the plasma accesses the high recycling and, subsequently, detached divertor regimes, the power deposited on the divertor plate decreases (in the case of the IR thermography under the detection limit of the JET diagnostic). It is also important to note that the power associated with the potential energy of the electron-ion pairs that recombine at the plate (in this case less than 0.5 MW at each divertor) also decreases as detachment proceeds and the ion flux decreases, particularly at the inner divertor.

The detachment process in L-mode is also simultaneous with a movement of the radiation away from the divertor and, at the latter stages of plasma detachment, the radiation is concentrated in the vicinity of the X-point. This is clearly seen in the tomographic reconstructions for the same L-mode density ramp (Fig. 22). However, as indicated also in this figure the concentration of impurities, as given by Z_{eff}, does not increase dramatically when detachment sets in. This observation is consistent with recent results from a multi-machine radiation database scaling [42], which show that the level of Z_{eff} in the main plasma is correlated to the level of radiation and the plasma density with very little influence of the regime of the divertor (i.e. high recycling or detached) during the experiment.

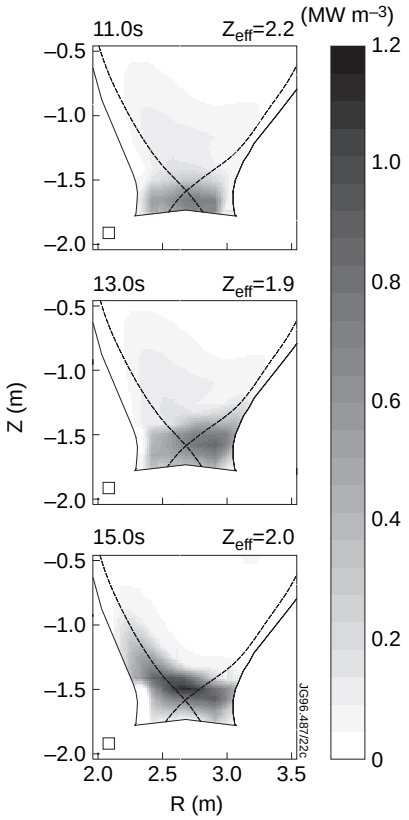

Fig.22: Bolometer reconstruction profiles for three phases of the L-mode density ramp in Figs. 16 and 17. At the onset of detachment the radiation peak moves away from the divertor towards the X-point. In spite of this, the Z_{eff} values do not increase significantly during this phase. The box shown in the bottom left hand corner indicates the mesh size used for the reconstruction.

A distinctive feature of L-mode detached plasmas is the occurrence of the so-called divertor oscillations [26]. These oscillations appear when the main plasma density is in the region of 4.0-6.0 10^{19} m^{-3} and the additional heating power exceeds 3.5 MW. At higher input powers the discharges undergo a transition to the H-mode regime and the situation becomes more complicated by the presence of ELMs. Once the density goes through these values, the oscillations disappear and the evolution towards detachment follows in a similar way to the Ohmic discharges. The general behaviour can be clearly seen in Fig. 23 for a L-mode unswept discharge, as large amplitude oscillations in the divertor ion saturation current and divertor D_α photon flux which cease above a certain main plasma density.

Fig. 24 shows the characteristic observations during divertor oscillations : periods of very low ion fluxes simultaneously at both the inner and outer divertor strike zones followed by large peaks in the ion fluxes with a repetition rate of approximately 10Hz. During the low ion flux phase, the inner divertor D_α decreases while the outer divertor D_α increases to make the distribution more symmetric between the strike zones. At the same time, the CII emission from the divertor target plate is strongly reduced (as shown in the contour plot in Fig. 24) and the radiated power in the vicinity of the strike zones decreases and increases near the X-point. As

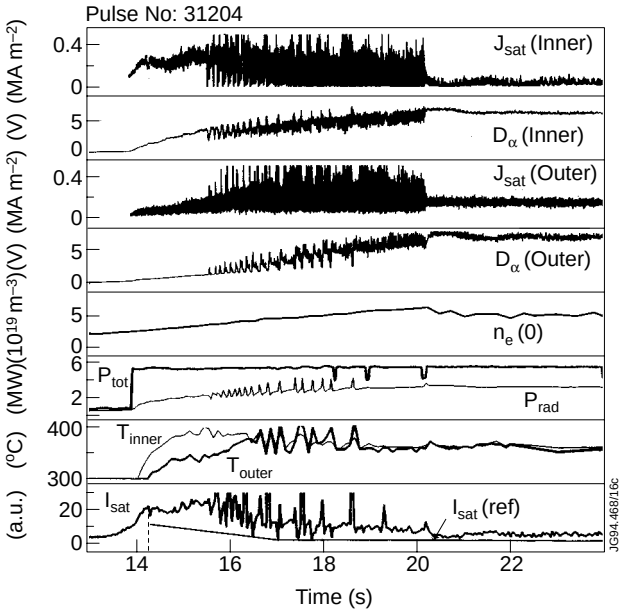

Fig.23: Main plasma and divertor parameters for an L-mode discharge in which the level of detachment was controlled by the feed-back of the gas fuelling level on the measured ion flux to the inner divertor (bottom trace). Note the large scale oscillations in the ion flux and divertor D_α emission before detachment starts.

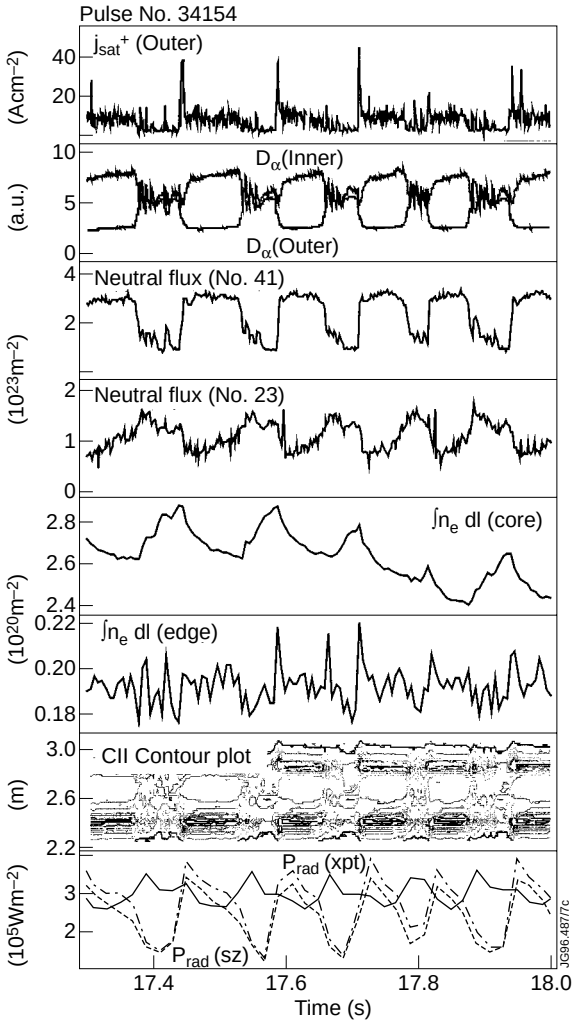

Fig.24: Behaviour of divertor and core plasma parameters during bi-stable divertor behaviour. Shown from top to bottom are the ion flux to the divertor, divertor D_α emission, neutral fluxes under the divertor, line integrated density in the main plasma and at the edge, CII emission from the divertor and radiated power from three Bolometers channels (SZ looks near the divertor inner and outer strike points and XPT looks near the X-point).

the ion flux decreases, the neutral flux under the inner strike zone (gauge #41) also shows a large drop while, at the private flux region (gauge #23) the neutral flux increases.

These oscillations are not only seen at the divertor but also affect the plasma parameters at the outer regions of the core plasma. During the low ion flux phase, there is a significant increase in the core plasma density and a decrease in the edge plasma density, as deduced by using two interferometer chords viewing different regions of the plasma. The density increase during the low ion flux phase is also measured by the LIDAR Thompson scattering diagnostic and appears to be localised to the outer regions of the main plasma leading to the formation of a hollow

density profile. Measurements of the electron temperature profile at the outer edge of the main plasma from an ECE heterodyne radiometer diagnostic are shown in Fig. 25. As the plasma density rises in the edge of the core plasma, the electron temperature falls sharply in the outermost 20 cm (r > 0.7a), this fall appearing to propagate from the plasma edge towards the centre. The electron temperature profile contracts during the low ion flux phase (labelled as 0.00ms) and recovers over a period of 16 ms, after which the divertor is fully attached. By further increasing the main plasma density with gas fuelling, the oscillation frequency decreases until they cease (see Fig. 23). Beyond the density window over which the oscillations occur, the divertor plasma can be driven further into detachment to eventually reach the density limit. The oscillations are observed in the density ramp up (strong gas puff) to detachment and ramp down (weak or no gas puff) and, hence, are **not** due to a fuelling effect. It is also interesting to note that these oscillations have also been induced during experiments in which neon is injected in short bursts into the divertor region, but that they are not generally observed during vertical plate and reversed toroidal field discharges.

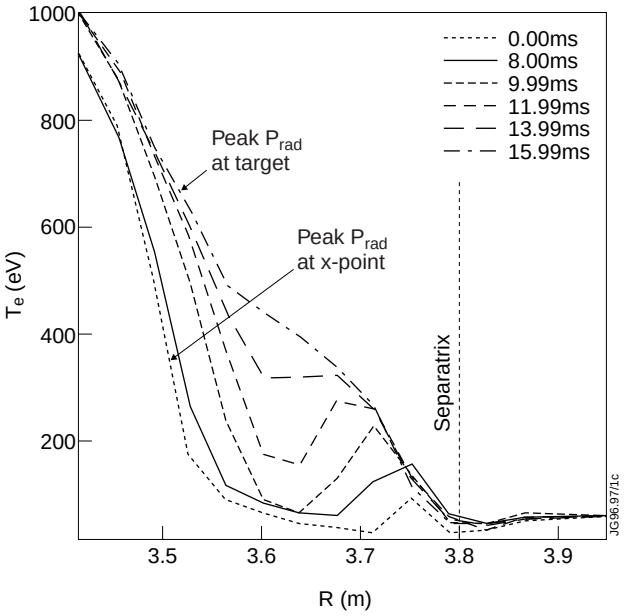

Fig.25: Measurements of the electron temperature profile from ECE at the edge of the main plasma during the bi-stable behaviour of the divertor plasma.

Given that the occurrence of the oscillatory divertor behaviour requires a minimum level of additional heating power and main plasma density, we believe that the observed phenomena are caused by impurity production from the divertor target. A possible interpretation of the observation is as follows : during the high ion flux phase carbon production reaches a maximum, this leads to the radiation moving above the X-point and, hence, a sharp decrease of the power that crosses the separatrix. After this period, the plasma is effectively totally detached from all material surfaces and the impurity production decreases, leading to a decrease in the radiation and to the re-attachment. The exact reasons as to why the MARFE becomes stabilised around the X-point when the density is increased further and the oscillations cease is not understood.

Similar observations of oscillatory divertor behaviour have also been reported in ASDEX-Upgrade [43, 44]. In that case, the oscillatory behaviour was attributed to the gas feed-back system which reacted to the increase in main plasma density as the MARFE moved up to the X-point region. In JET, the gas fuelling feed-back system has an overall response time greater than 150 ms and, therefore, is too slow to react at oscillation frequencies that are typically observed. Transport phenomena in the scrape-off layer will occur on the timescale of few milliseconds, i.e. much more rapidly than the divertor oscillations. The timescale of the oscillations is more

consistent with diffusive processes at the edge of the core plasma. While the mechanism proposed above may account for many of the experimental observations, it is clear that the phenomena associated with the self-sustained divertor oscillations are extremely complex and involve changes in plasma parameters in both the divertor and core plasma regions.

Despite the occurrence of such oscillations, the regime of divertor detachment in L-mode, in which the inner divertor is totally detached while the outer one is partially detached, has proven to be a fairly robust regime. It has been possible to keep the divertor in this regime by means of feed-back control of the gas puff on the level of ion flux to the inner divertor [13]. In this experiment (Fig. 23), the plasma was driven to detachment by feed-forward control of the gas puff and subsequently maintained in the detached state by controlling the gas puff (increasing or decreasing it) as the divertor flux increased (attachment) or decreased (too detached) with respect to a reference ion flux request waveform.

3.3. H-mode Discharges

The response of the divertor to the increase of main plasma density during H-mode discharges is significantly different from that described above for Ohmic and L-mode discharges, due to the occurrence of the ELMs associated with this confinement regime. As is observed in most divertor tokamaks, the ELM characteristics change as the rate of fuelling of the plasma is increased with gas puffing and the ELMs become more frequent with increasing fuelling rate [45,46].

The typical behaviour observed during H-mode discharges is shown in Fig. 26.a & 26.b for a series of discharges with increasing gas fuelling at the same input power. As the gas puff rate increases, the main plasma density increases and the ELMs, as seen by the divertor D_α emission, evolve from being large and sparse (Type I) to higher frequency and smaller ELMs. Beyond a certain level of gas fuelling rate, the main plasma confinement deteriorates (for this series of discharges it corresponds to the density reaching the Greenwald density [47], but it is usually lower) and the discharge falls back into L-mode, with the corresponding decrease in main plasma density [48]. The typical level of total radiation reached at this point is only approximately 50% of the input power, which is clearly insufficient for the levels foreseen to be required in next step devices such as ITER [2]. This fact has led to the exploration of a similar regime to this one, but with the use of extrinsic impurities, which allow higher radiation fraction together with reasonable levels of energy confinement in the main plasma [11, 49]. This regime is the subject of separate studies [11] and we will only discuss it briefly in this paper.

The pattern of increasing divertor D_α emission, subdivertor neutral pressure and ion flux up to high recycling followed by roll-over and detachment, as seen in Ohmic and L-mode regimes, is also observed in the ELMy H-modes, albeit between the ELM events. This is highlighted in Fig. 26.b for the discharges described above, where the ion flux and divertor D_α emission between ELMs increases with the increase of gas puff and then rolls over (while the divertor D_α emission continues to increase). It can also be seen that at the ELM events reattachment occurs and large

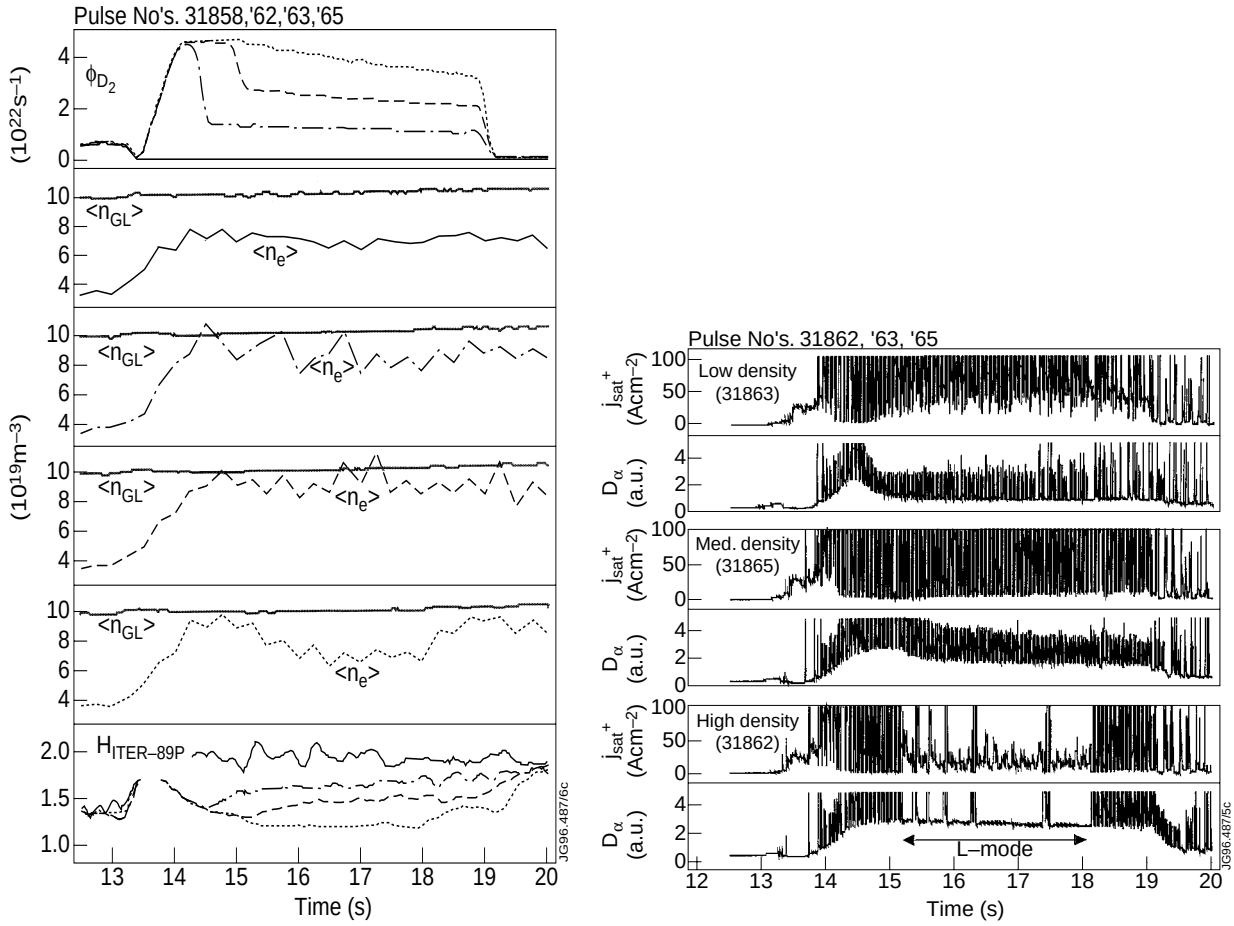

Fig.26:.a Main Plasma parameters for a gas fuelling scan in 2.5MA ELMy H-mode conditions showing the loss of confinement (transition to L-mode) at the highest fuelling rate. In Figure 26.b. the ion flux measured at the outer divertor shows a decrease between ELMs, as the main plasma density increases, but not at the ELM event (detachment between ELMs but not at ELMs) typical of these discharges.

plasma fluxes to the target are measured (larger than 100 A/cm^2 along the field). Reattachment between ELMs can be eliminated, albeit at the cost of increasing the impurity content of the main plasma, if impurities are added to the gas fuelling of the discharge achieving the so-called impurity seeded H-mode or CDH-mode [11,49]. In these discharges the divertor remains detached throughout the H-mode phase and larger radiative losses can be achieved. Fig. 27 shows the ion flux profiles measured at the divertor for three characteristic examples of (a) H-mode without gas fuelling, (b) Deuterium gas fuelled H-mode and (c) impurity seeded (Nitrogen) H-mode. The unfuelled discharge has infrequent ELMs while the gas fuelled H-mode has a very low ion flux in-between ELMs with large fluxes at the ELMs (detachment between ELMs and attachment at the ELMs). The Nitrogen seeded discharge has very high frequency ELMs (similar to the gas fuelled case) but the divertor remains detached throughout.

This change of the characteristics of attachment/detachment with the ELMs is corroborated by measurements of the electron pressure in the SOL and at the divertor as shown in Fig. 28 for

the discharges of Fig. 27. While for the discharge without gas puff the electron pressure in the SOL is the same than at the divertor in between ELMs, for the gas fuelled discharge there is more than an order of magnitude pressure drop from the SOL to the divertor in between ELMs close to the separatrix. At the ELM event the pressure balance is restored indicating the reattachment of the divertor plasma. Similar pressure drops can be deduced for impurity seeded H-modes but in this case the divertor remains attached even at the ELM at least for the region close to the separatrix.

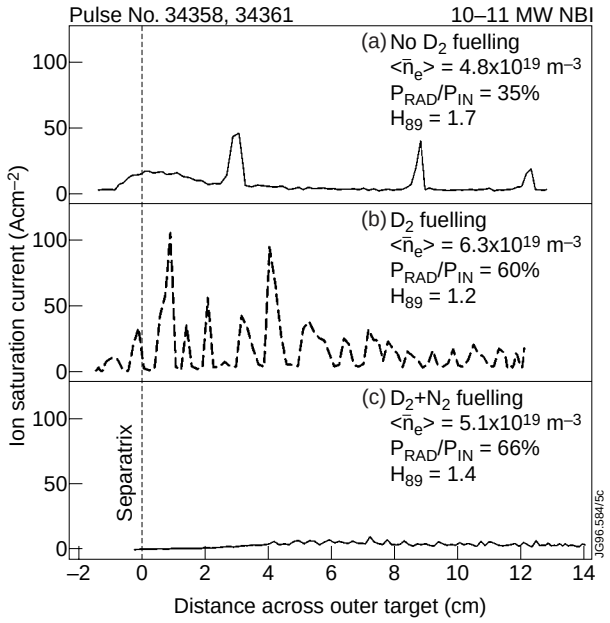

Fig.27: Measured ion flux profiles at the outer divertor target for three H-mode discharges : (a) No Deuterium fuelling, (b) Strong Deuterium fuelling and (c) Deuterium and Nitrogen Fuelling. Note the low values of the ion flux between ELMs (detachment) and high values at the ELMs (attachment) for discharge b). For the impurity seeded discharge the pertubations caused by the ELMs are very small and the divertor remains detached at the ELM events.

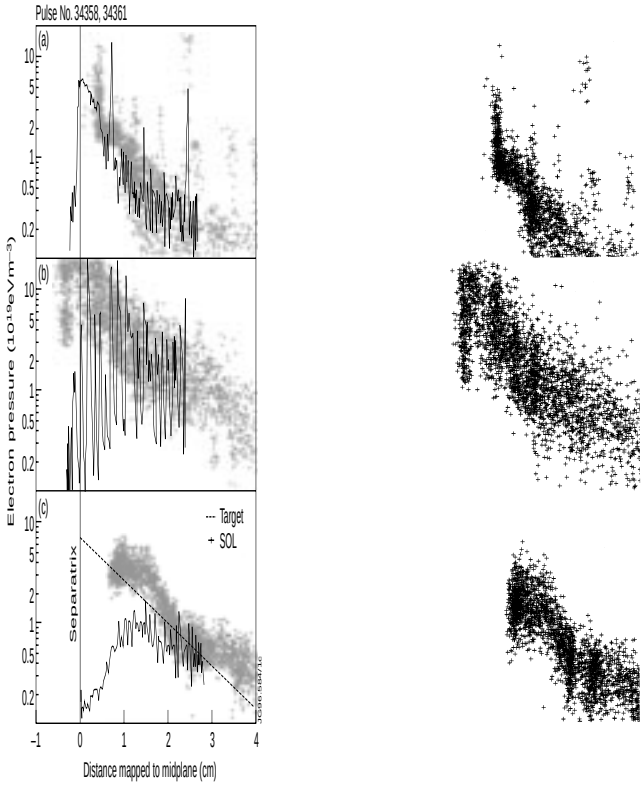

Fig.28: Electron pressure profiles in the SOL and at the divertor for the discharges in Fig. 27. Note the large pressure drop close to the separatrix between ELMs for discharge (b). In the case of discharge (c), there is detachment both between and during ELMs (note that the separatrix electron pressure is extrapolated from measurements futher out in the SOL).

Another characteristic observation at the inner divertor of this detached (between ELMs) /attached (at ELMs) regime is the appearance of the so-called “negative” ELMs. In this case, the level of D_α emission from the inner divertor decreases at the ELM, in contrast to the typical ELM picture [50] (see Fig. 29). This phenomenon has also been reported for high density regimes in DIII-D [6] and it can be explained by considering the effect of the energy pulse associated with the ELM on the detached plasma. As the ELM energy pulse arrives at the inner,

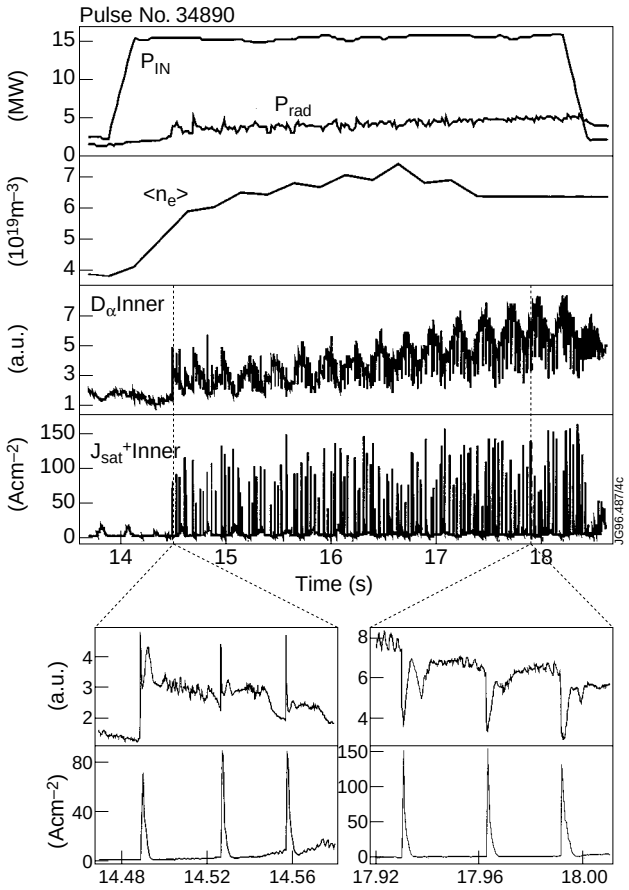

Fig.29: Main plasma and inner divertor parameters for a discharge in which a gas fuelling rate scan is performed in ELMy H-mode conditions. As the fuelling rate is increased with time the ELMs, as measured by the D_α emission from the inner divertor, evolve into "negative" ELMs, as detachment between ELMs starts. Note that at the ELMs the divertor reattaches again, as shown by the large measured values of the ion flux at the inner divertor.

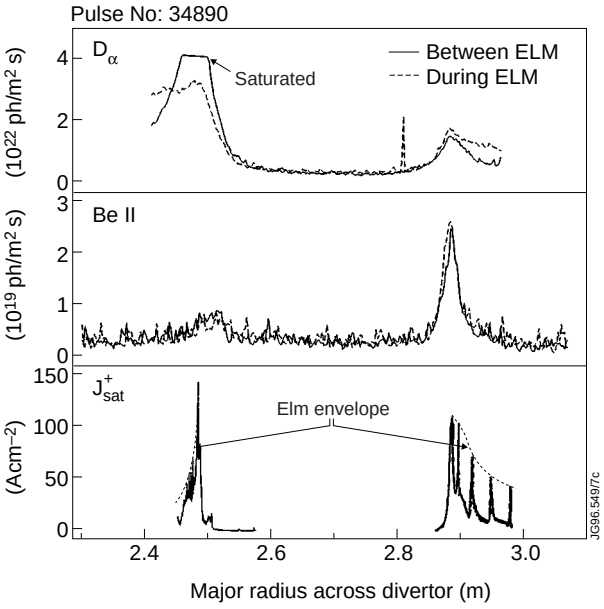

Fig.30: Divertor D_α, BeII and ion flux to the divertor between ELMs (full lines, note that the inner divertor D_α signal is saturated) and at the ELMs (dashed lines) showing the detachment between ELMs and reattachment at the ELM during the high density ELMy H-mode discharge of Fig. 29.

detached, divertor, the electron temperature increases from very low values between ELMs ($T_e \leq 5$ eV), hence, ionising the neutral gas confined in the divertor during the detached phase by charge-exchange and recombination, and causing the number of ionisations per D_α photon to increase. This process actually reduces the divertor D_α emission despite the increase of the ionisation in the divertor. This observation is illustrated in detail in Fig. 30 for a discharge with the Mark I Beryllium target, where the divertor D_α emission profile, Be II emission profile and ion flux to the divertor target are compared for a high density discharge with 15 MW of NBI (that of Fig. 29), where the inner divertor is detached while the outer remains attached. Between ELMs, the inner divertor D_α emission signal is saturated and decreases at the ELM ("negative" ELMs), while it increases at the outer divertor in the normal fashion. However, for both divertors the ion flux increases at the ELM event. This confirms that the inner divertor is detached

between the ELMs and reattaches at the ELM. It is important to remark that no significant increase of the BeII emission is observed at either divertor at the ELM, with the levels being negligible for the inner divertor. This lack of Beryllium emission from the inner divertor is consistent with a very low divertor temperature even at the ELM since, as it has been established experimentally in JET, Beryllium is produced by physical sputtering processes which have a very low energy threshold (10 eV-20 eV incident ion energy, depending on the degree of oxidation) [51]. Consequently, as soon as the electron temperature increases beyond 5 eV a significant BeII emission would be expected (see Section 5 for a more detailed discussion on this topic).

4. EFFECTS OF DIVERTOR GEOMETRY, WALL CLEARANCE, TOROIDAL FIELD DIRECTION AND DIVERTOR PUMPING ON DIVERTOR DETACHMENT

4.1. Effects of the divertor geometry and wall clearance on plasma detachment.

A systematic study has been performed at JET to understand the effect of divertor geometry on the onset and stability of plasma detachment. During this study, it was found that there is an additional factor that affects detachment at least as much as the divertor geometry : the clearance between the separatrix and the nearest material surface. This fact somewhat complicates the study of divertor geometry effects as, in changing the divertor geometry, the clearance from the wall is unavoidably varied too. Hence, we will firstly discuss the observed effect of a controlled change of the wall clearance on plasma detachment with fixed divertor geometry before describing the effect of the divertor geometry on detachment.

In Ohmic discharges, it has been found that discharges which are well separated from the walls (where approximately the 5 cm line in the SOL, mapped to the outer midplane, intersects a material surface outside the divertor) have a higher density threshold for detachment and density limit by about 35% [26], than those which have less clearance from the walls (2.5 cm at the mapped to the outer midplane). The proximity of the walls also affects the split between the bulk and divertor+X-point radiation, which is about 1/3 bulk and 2/3 divertor+X-point for high clearance discharges, while it is 1/2 bulk and 1/2 divertor+X-point for low clearance discharges. A comparison of two identical discharges, except for the clearance to the top of the torus, is shown in Fig. 31a & 31b, exhibiting the typical features illustrative of the influence of wall clearance on the main plasma parameters and divertor detachment.

The influence of wall clearance in L-mode and H-mode detachment is found to be much weaker (10-15 % difference in main plasma density to achieve detachment) [26]. A possible explanation of this effect is that the L-mode profiles tend to broaden very strongly at the beginning of detachment, as discussed in section 3.2 and, hence, in all configurations there is some degree of interaction with the walls for these discharges. In the case of H-mode detachment, the same argument would apply due to the interaction of the ELMs with the main chamber walls.

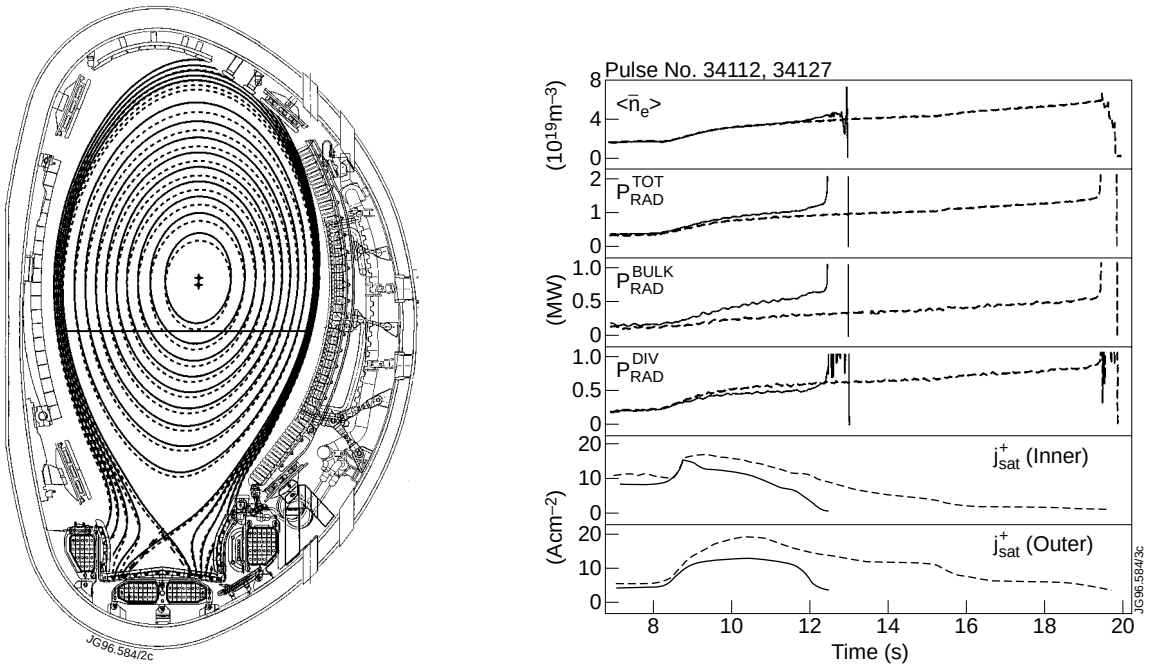

Fig.31: a. MHD equilibrium for two identical Ohmic discharges with different wall clearance to the top of the machine. In Fig. 31.b. the main discharge and divertor parameters (full line low clearance, dashed line high clearance) show the lower detachment threshold and density limit for the discharge which has strongest interaction with the walls. It is also evident that the proportion of bulk plasma radiation is higher for the low clearance discharge.

Because of the unavoidable change of wall clearance with divertor geometry in the experiments, in particular with the variation of the divertor flux expansion, we have divided the study of the influence of divertor geometry on detachment into two separate sets of experiments. Fig. 32 shows the MHD equilibria reconstructions for the four typical configurations used in this study.

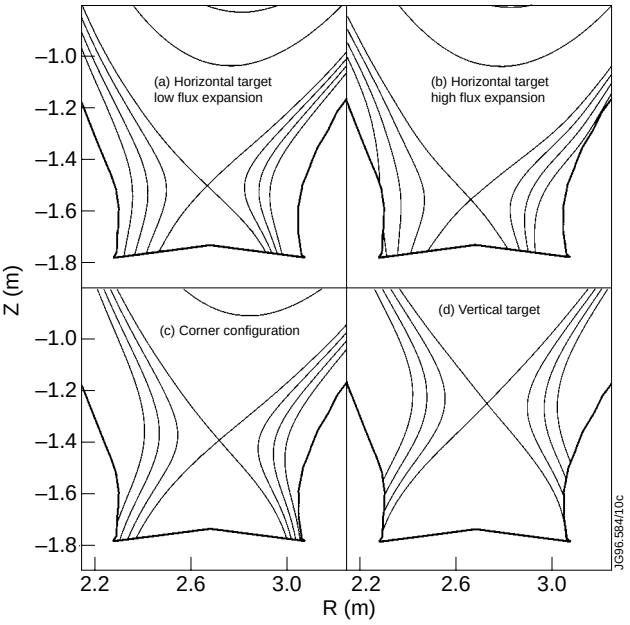

Fig.32: MHD equilibrium reconstructions of typical configurations used for the studies of the influence of the magnetic configuration on plasma detachment. The flux surfaces correspond to a spacing of 1 cm at the outer midplane.

4.1.1. Divertor geometry variation with "fixed" magnetic configuration : vertical/horizontal comparison at low perpendicular flux expansion

There are no substantial differences in the access to detachment for similar discharges in horizontal and vertical divertor configurations. Detachment occurs at similar plasma density, gas fuelling rate and radiation levels for both cases in Ohmic, L-mode and H-mode regimes.

This observation is in contrast to expectations from 2D modelling calculations of the closure to neutrals of both configurations [52, 53] and this discrepancy is believed to be due to the existence of by-pass leaks for neutrals from the divertor to the main chamber (which are present in the experiment and not in the original calculations) and the possible existence of an inwards particle pinch in the SOL [54]. Both factors, when taken into account, modify substantially the neutral reionisation pattern and the calculated divertor closure and therefore the dependence of detachment on the divertor geometry. For vertical plate discharges, with forward field detachment seems to take place more symmetrically between the inner and the outer divertor, while in the horizontal plate the inner divertor tends to detach first, as the density is increased (further discussed in section 6).

Detailed comparison of the ion flux profiles at the divertor plate for Ohmic and L-mode discharges shows that the profiles are somewhat steeper (in outer midplane co-ordinates) when the separatrix is located at the lower part of the vertical plate than those of the horizontal plate divertor. However, when the separatrix is located in the upper part of the vertical plate they are very similar to those on the horizontal plate (Fig. 33). This trend is expected from modelling calculations [53, 55] as a consequence of the preferential ionisation of neutrals at the separatrix in the case of vertical plate divertors, although the size of the effect is smaller in the experiment than from the modelling calculations. The differences in the temperature profiles between horizontal and vertical divertors are very small and are identical within the experimental errors. These temperature profiles are very flat for the high

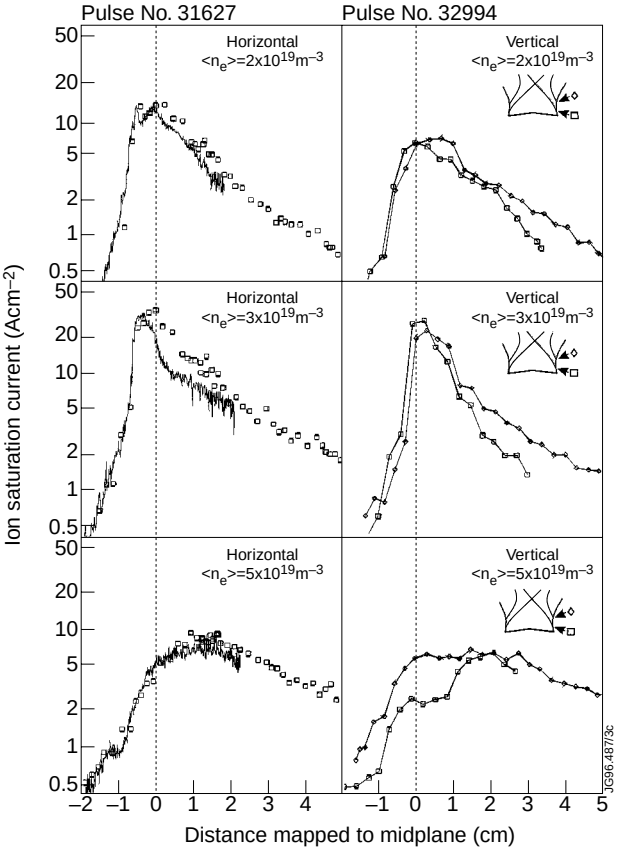

Fig.33: Ion flux profiles at the outer divertor for two Ohmic discharges, one on the horizontal and other on the vertical divertor plate during the low recycling, high recycling and detached phases. Several probes (Triple probes (full line) and single probes (symbols)) are overlaid together on the horizontal plate discharge, while for the vertical plate they are plotted with different symbols because of the effects of separatrix location on the vertical plate as discussed in the text.

recycling phases of both divertor configurations. However, as discussed insection 3.1.3, it must be stressed that the electron temperature measurements with Langmuir probes under these conditions become questionable.

A characteristic behaviour of vertical plate divertor discharges, not found for discharges on the horizontal plate, is the sensitivity of detachment to the exact position of the strike point on the vertical plate [53]. When the divertor strike points are swept across the horizontal divertor plate, no noticeable difference is seen in the ion flow profiles measured with probes at different positions in the target (for instance see Fig. 33 for an Ohmic discharge where the measurements of several probes are overlaid). In this case, the profiles maintain the same shape and degree of detachment as the strike point moves across the divertor target. However, when the strike point is swept across the vertical plate, the profiles of ion flux and the degree of detachment may change considerably, depending on the position of the strike point. While the divertor is detached when the strike point is at the lower part of the vertical plate (near the corner between vertical and horizontal plate), the plasma re-attaches as the strike point moves to the upper part of the vertical plate (Fig. 34 for an L-mode example). This strong dependency of detachment on the strike point position on vertical plate is consistent with expectations of the estimated divertor closure for neutrals in both geometric configurations on the vertical plate [53]. However, it is important to note that the degree of detachment achieved on the any zone of the vertical plate is never larger than that obtained on the horizontal plate, and this goes against our general expectations and is not yet fully understood.

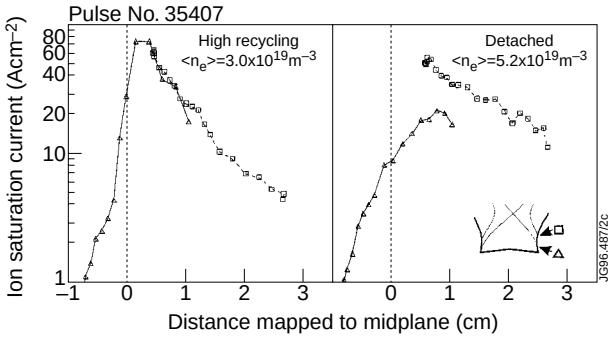

Fig.34: Ion flux profiles at the outer divertor, during an L-mode density ramp discharge in the high recycling and detached divertor phases. Profiles are shown for two probes on the vertical plate (squares refer to the upper part of the vertical plate, triangles lower part of the vertical plate). The degree of detachment differs substantially at each probe position, being much larger when the separatrix is located in the lower part of the vertical plate.

In summary, vertical and horizontal divertor discharges display very similar characteristics in the approach to detachment and operation on the vertical plate does not lead to a larger operating regime for detached plasmas, in contrast to original expectations from code calculations. While there is evidence that part of this behaviour can be attributed to the existence of by-passes for neutrals to escape from the divertor into the main chamber and SOL plasma perpendicular transport processes, the similarities between vertical and horizontal divertor are not yet fully understood.

4.1.2. Divertor magnetic geometry variation on horizontal plates

The strongest effect of the divertor magnetic geometry on detachment seen in the experiment is associated with the increase of flux surface separation (flux expansion) at the divertor target. For Ohmic discharges, it has been found that discharges with lower flux expansion (inner divertor 4.9, outer divertor 2.1) have a threshold density for detachment and a density limit which is about 30-40% larger than that of a similar discharge with higher flux expansion (inner divertor 6.3, outer divertor 3.2) (Fig. 35). The open question regarding this comparison is the fact that the clearance from the walls (particularly to the inner divertor wall and to the top of the vessel) is significantly decreased when the divertor flux expansion is increased (from 5 cm at the midplane for low flux expansion to 2.5 cm for large flux expansion). This change in clearance may be the dominant effect that accounts for the observations, rather than the flux expansion itself. The split between divertor radiation and main plasma radiation seems to be consistent with the wall clearance being the dominant factor : for low flux expansion discharges the radiation split is approximately 1/3 bulk radiation and 2/3 divertor radiation, while for high flux expansion the split is 1/2 bulk to 1/2 divertor radiation. This observation is in agreement with those from discharges in which just the wall clearance is changed without needing to include any additional effect of changing the divertor geometry. Measurements of the carbon radiation in the visible and VUV wavelengths from the inner divertor indicate that the contribution of carbon to the measured radiation dominates as the clearance to the inner divertor wall (see Section 5 for a detailed discussion).

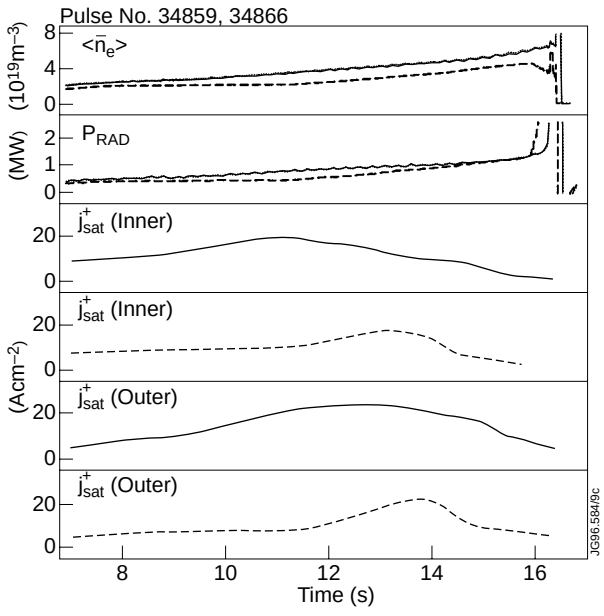

Fig.35: Plasma density, total radiation and ion flux to the inner and outer divertor for two Ohmic horizontal divertor discharges with low flux expansion (full line) and high flux expansion (dashed line).

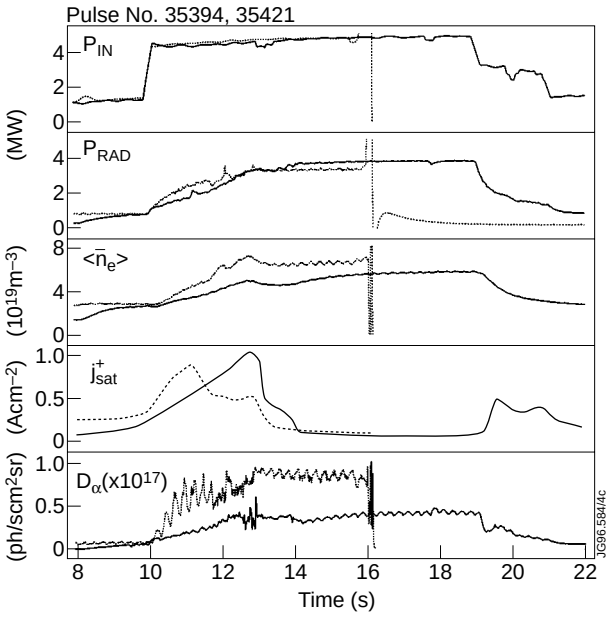

Fig.36: Input power, total radiation, plasma density, ion flux and D_α to the inner divertor for two L-mode horizontal divertor discharges with low flux expansion (dashed line) and high flux expansion (full line).

A similar behaviour is found in L-mode and H-mode discharges, although the differences between configurations are somewhat smaller (Fig. 36). The reason is likely to be associated with a stronger interaction with the walls for any configuration caused by the ELMs or the flattening of the SOL profiles in the approach to detachment for L-mode density ramps.

4.2. Effects of the toroidal field direction on divertor detachment

Dedicated experiments have been carried out in JET to compare the effect of the toroidal field direction on detachment. Reversed toroidal field Ohmic and L-mode discharges tend to display more symmetric divertor parameters between the inner and the outer divertor [56] for, otherwise, identical core plasma parameters. This leads, in horizontal divertor high clearance configurations, for detachment to take place more symmetrically at the inner and the outer divertors for the reversed field discharges. However, in contrast to forward field discharges which are fairly stable, reversed field discharges tend to form a MARFE in the main plasma as soon as detachment starts at the outer divertor. The trend of the radiation to escape the divertor in reversed field discharges had been observed previously in the JET 91/92 experimental campaign [57] and in ASDEX-Upgrade [44,58] and JT-60U [12] and it is not well understood. A comparison of two Ohmic discharges, identical but for the toroidal field direction, is shown in Fig. 37. In general, it is observed that, for similar main plasma densities, the Z_{eff} measured in forward and reverse field discharges is similar and, hence, increased impurity levels in the main plasma for reversed field discharges (as proposed in [58]) can be ruled out as the explanation for this behaviour in the JET experiments.

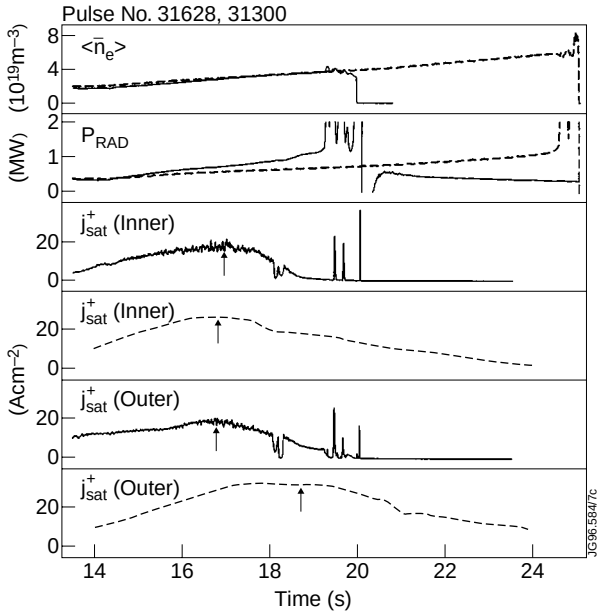

Fig.37: Plasma density, total radiation, and ion flux to the inner and outer divertor for two Ohmic horizontal divertor discharges with forward field (dashed line) and reversed field (full line).

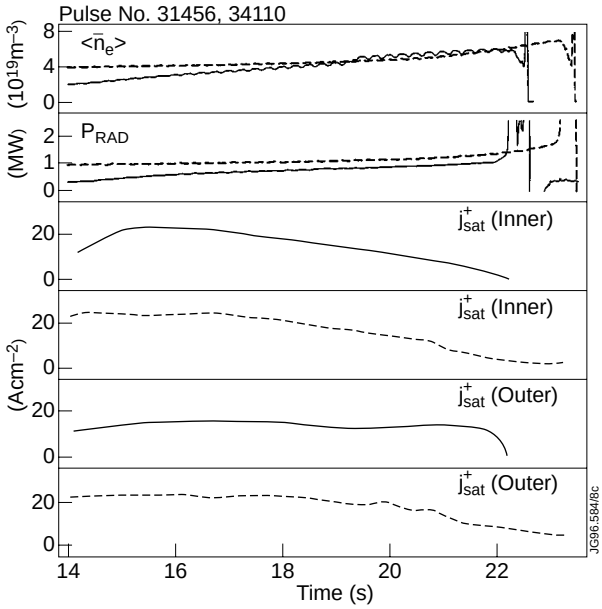

Fig.38: Plasma density, total radiation, plasma density and ion flux to the inner and outer divertor for two Ohmic discharges in corner configuration with forward (dashed line) and reversed field (full line). Note the unstable but more asymmetric approach to detachment of the reversed field discharge.

The more symmetric approach to detachment in reversed field discharges is, however, not seen in all magnetic configurations. In particular, vertical plate and corner configurations are more symmetric in the approach to detachment with forward direction of the field. Fig. 38 shows two discharges in corner configuration with different directions of the toroidal field. However, the unstable approach to detachment of the reversed field discharges is clearly seen and, hence, does not depend on details of the magnetic configuration but principally on the direction of the toroidal field.

L-mode discharges behave similarly to Ohmic ones with respect to the dependence of detachment on toroidal field direction. Therefore it has not been possible to obtain steady state L-mode detached discharges with reversed field. Although the instability of divertor detachment in the reversed field case is not understood, it highlights one of the major disadvantages of operating the JET device with this direction of the toroidal field. Although the power load may be more symmetric for reversed field in some configurations, the stability of high density operation is significantly compromised, which, therefore, limits access to regimes with low power loading on the divertor target.

4.3 Effects of divertor pumping on divertor detachment

By using the cryopump installed in the JET Mark I divertor it has been possible to study the effect of active divertor pumping on detached plasmas. The cryopump is situated at the outer side of the divertor and it has a measured effective pumping speed of 160 m^3/s [16]. The use of the cryopump has many beneficial effects with respect to the general wall conditioning of the machine but has no significant effect on detachment in Ohmic and L-mode discharges. For discharges with the cryopump at liquid Helium temperature, higher gas fuelling rates must be used in order to increase the main plasma density to values similar to those obtained in discharges where the cryopump is warm, as expected. However, the plasma density at which detachment takes place and the density limit are found to be very similar for discharges with/without cryopumping. For H-mode discharges, the influence of divertor cryopumping is more significant, as in this case confinement effects at high densities play a dominant role [48]. Examples of this influence will be discussed in more detail in Section 6.

Despite the gross similarities between discharges with and without divertor cryopumping, subtle effects of the cryopump on plasma detachment have been observed for Ohmic and L-mode discharges. When the strike point of a detached horizontal divertor discharge is moved towards the corner of the divertor, where the particle removal by the cryopump is at a maximum [16], the plasma attaches again (Fig. 39). This effect proves experimentally the importance of maintaining a large neutral pressure and low electron temperature in the divertor to achieve plasma detachment.

Finally, it is very important to note that since the neutral pressure in the subdivertor module remains high during plasma detachment, active pumping can be very effective, even more so

than for the high recycling regime (which has a lower neutral divertor pressure). Hence, in terms of convection in the SOL and pumping, the detached divertor regime compares very favourably with the high recycling regime.

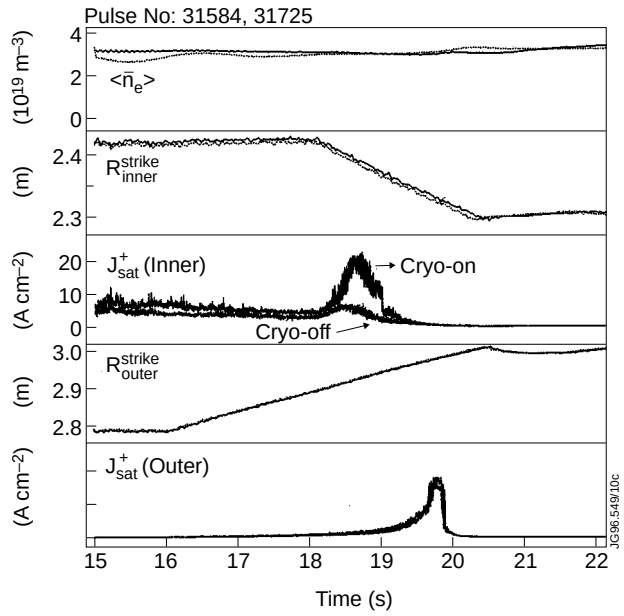

Fig.39: Plasma density, strike point position and ion flux to the inner and outer divertor (at the corner of the horizontal plate) for two identical discharges with (full line) and without (dotted line) divertor cryopumping. Note that the ion flux to the inner divertor is larger for the case with the cryopump on and that the discharge with the cryopump off is partially detached at the inner divertor.

5. DIFFERENCES IN DETACHMENT BETWEEN CARBON AND BERYLLIUM DIVERTOR PLATES AND IMPURITY BEHAVIOUR DURING DETACHED DIVERTOR PLASMAS.

Detached divertor experiments have been carried out in the JET Mark I divertor with two different divertor plate materials : Carbon and Beryllium. However, the remaining plasma facing components remained unchanged throughout the Mark I experimental campaign. These first wall components are mainly made of carbon (except for the ICRH antenna Faraday screens which are made of Beryllium) but Beryllium evaporations are routinely performed at JET that covers the plasma-facing surfaces with a layer of Beryllium. The general behaviour of discharges with both divertor target materials are very similar and within the experimental uncertainties of the experiments carried out with either divertor material [59]. Fig. 40 compares two steady-state L-mode detached plasmas on the carbon target and on the beryllium target. The reason for the similarity between the two cases is due to the fact that, regardless of divertor target material, the radiation is dominated by Carbon coming from redeposited layers at the divertor target and the plasma facing first wall components [60].

There is a clear experimental difference in the behaviour of beryllium and carbon impurities, which is due to the different generation mechanism that produces these impurities. In all the

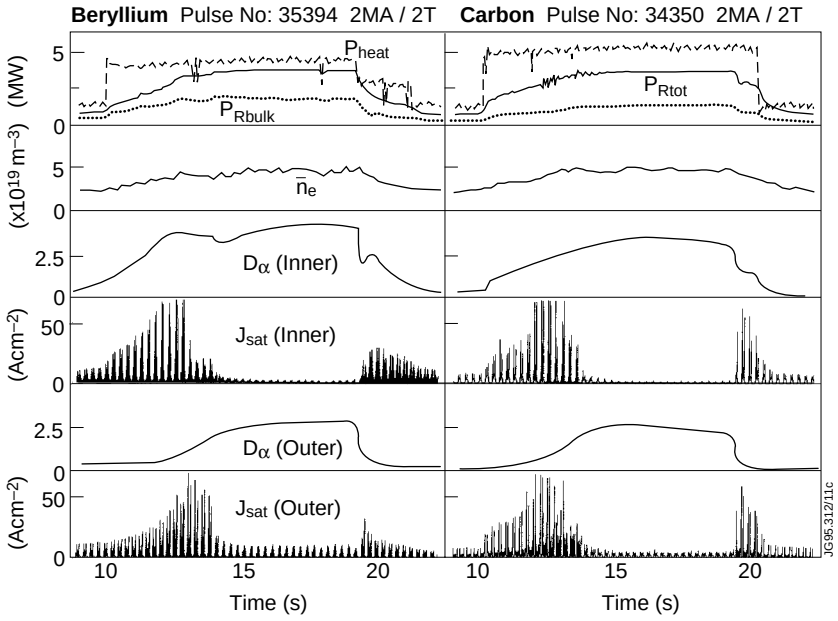

Fig.40: Input power, total radiation, plasma density, D_α emission and ion flux to the inner and outer divertor for two L-mode discharges on the horizontal divertor with Beryllium and Carbon targets.

experiments performed to achieve divertor detachment, it is observed that the beryllium visible emission from the divertor decreases to negligible levels as the density is increased to achieve the high recycling regime in the divertor. On the contrary, carbon emission from the divertor either decreases slightly or even increases (high flux expansion configurations) with increasing main plasma density. This different behaviour can be understood on the basis of the impurity production mechanism which involves only physical sputtering for beryllium, while for carbon chemical processes also play a role [51]. Chemical sputtering is particularly important at low divertor temperatures (typical of high recycling and detached divertors) where physical sputtering is negligible. Fig. 41 shows observations of the beryllium and carbon emission from visible spectroscopy at the outer divertor for two discharges (Ohmic and L-mode) on the beryllium target which display the typical behaviour described above.

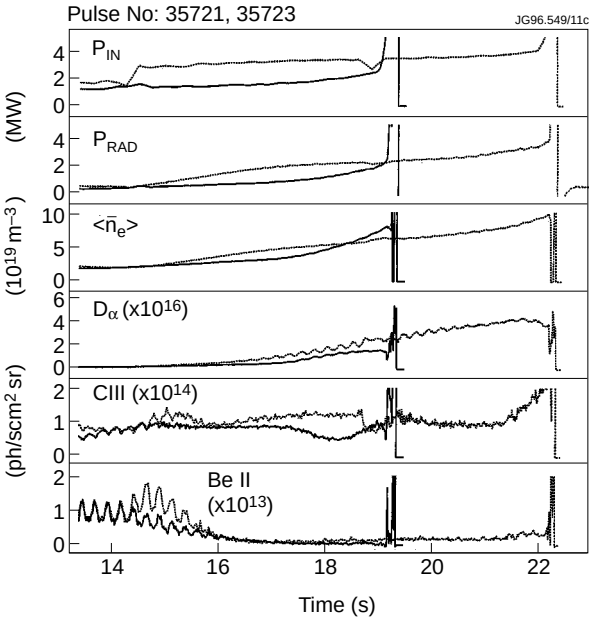

Fig.41: Input power, total radiation, plasma density, D_α emission, CIII emission and BeII emission from the outer divertor, for an Ohmic (full line) and an L-mode discharge (dotted line) on the horizontal Beryllium target. Note that while the Beryllium emission decreases with increasing density the carbon emission stays approximately constant (or even increases) during the density ramp up to the density limit.

The spatial origin of the chemically produced carbon has not been precisely identified (horizontal divertor target, side plates or inner wall), but it is seen to depend strongly on the magnetic configuration. Fig. 42 shows two L-mode steady state detached plasmas on the horizontal plate with low flux expansion (high wall clearance) and with high flux expansion (low wall clearance). The measured intensity of the carbon emission from the divertor is larger for the discharge with high flux expansion (low wall clearance). These differences highlight once again the strong influence of the interaction of the plasma with first wall structures other than the divertor plate itself and whose effect may be as important as that of the divertor target in the experiment.

The same difference between high clearance and low clearance discharges is reflected in the split of the divertor radiation between the different species, as measured with VUV spectroscopy [60]. Fig. 43 shows this effect for a series of Ohmic discharges with different wall clearance (high flux expansion with low wall clearance and low flux expansion with high wall clearance). One can see that for the discharges with high wall clearance the ratio of carbon to hydrogen radiation falls continuously as the density increases, to values of about 0.3. In contrast, for discharges which have low wall clearance this ratio falls initially and then stays approximately constant at a value of 0.9 until the discharge ends in a density limit disruption. For L-mode and H-mode discharges similar trends are found, but the differences between the configurations are smaller in accordance with the observations presented in section 4.

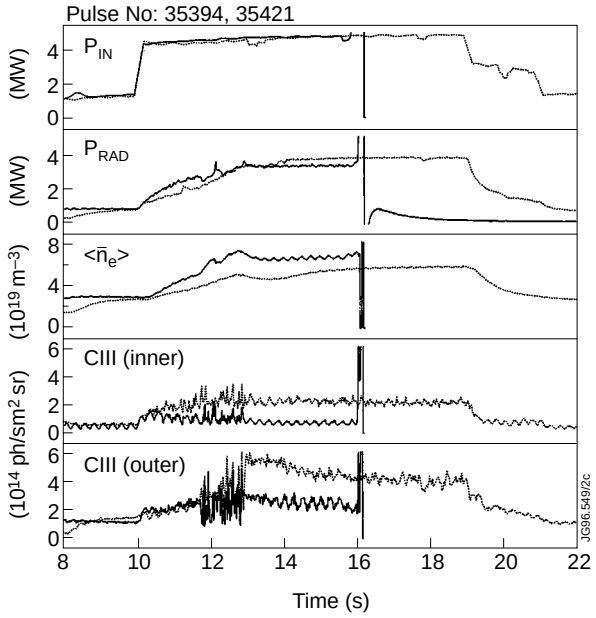

Fig.42: Input power, total radiation, plasma density, CIII emission from the outer and inner divertor for two L-mode steady state detached plasmas, with low (full line) and high (dashed line) flux expansion at the horizontal divertor.

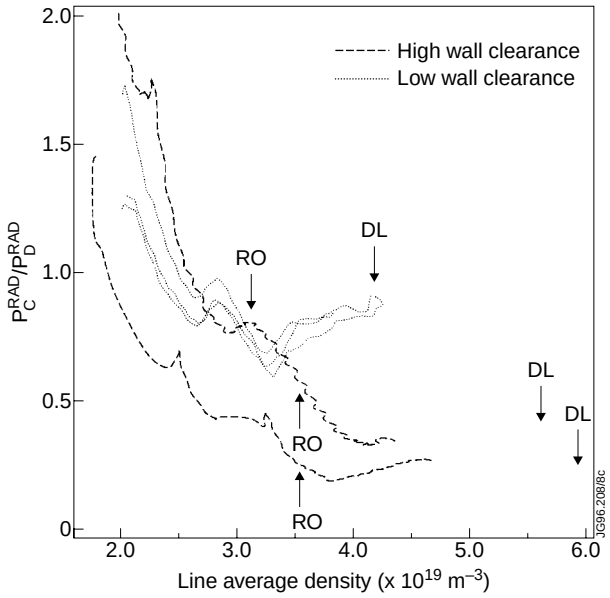

Fig.43: Measured ratio of Carbon to Deuterium radiation from the inner divertor for a series of Ohmic discharges on the horizontal divertor plate with low flux expansion (high wall clearance) and high flux expansion (low wall clearance) [60]. The densities at which the roll-over phase and the density limit is reached in these discharges is also indicated.

The simple picture of impurity contamination of the main plasma and its dependency on detachment seems not to be followed by the experiment. In a simple physical picture, one would expect that the impurity retention in the divertor would increase, as the main plasma density is increased and the high recycling regime is achieved. From the roll-over phase towards detachment, one would expect the impurity contamination of the bulk plasma to worsen, as the radiation moves from the divertor plate to the X-point. However, there is no clear experimental indication that this simple picture is reproduced. There is no significant impurity concentration increase in the main plasma with the onset of detachment and the movement of the radiation maximum from the divertor target to the X-point region. Fig. 44 shows this typical behaviour for an Ohmic and an L-mode discharge. The physical basis behind this unexpected behaviour can be understood in two ways : MARFE modelling [61], shows that impurities can be well confined in the radiating region by strong recirculating flows and, hence, the fact that the radiating region is close to or within the separatrix does not necessarily imply a large contamination of the main plasma; alternatively the impurity level in the main chamber may be determined by processes of interaction of the plasma with the main chamber walls that are not related directly to the divertor and, hence, the divertor regime does not have a major influence on the main plasma impurity concentration. The second line of argument is also in agreement with recent multi-machine scalings for radiative divertors [42] which show that Z_{eff} is linked to radiation and plasma density for every machine regardless of divertor regime (attached or detached). Although by using impurity seeding or changes in the edge electron temperature can shift the radiation distribution significantly, the robustness of the Z_{eff} scaling shows that impurities themselves are not strongly retained in the divertor for highly radiative regimes.

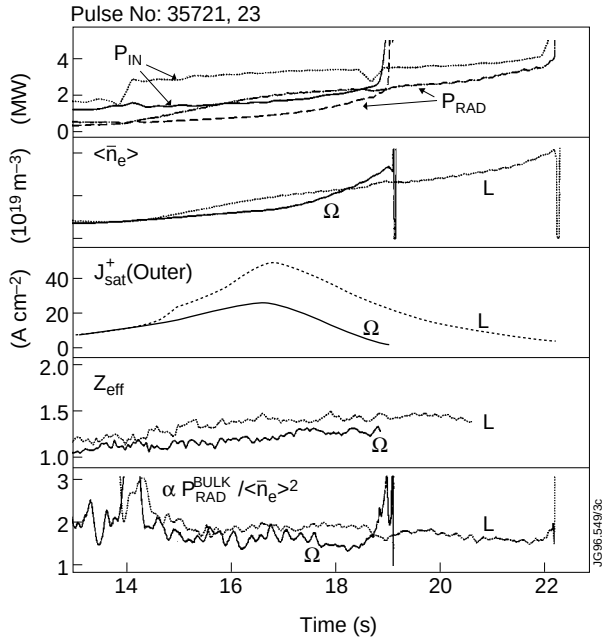

Fig.44: Input power, total radiation, plasma density, outer divertor ion flux, Z_{eff} and $P^{bulk}_{rad}/<n_e>^2$ (which should be proportional to Z_{eff}) for an Ohmic (full line) and L-mode discharge (dotted line) on the horizontal divertor plate.

6. THE DEGREE AND WINDOW OF DETACHMENT

In order to summarise and compare quantitatively many of the observations described in the previous sections, detachment has to be defined in a precise way. For this purpose we introduce the concepts of “degree of detachment” and the “detachment window”. These parameters will be based upon simple plasma edge models and the experimental measurements of the measured ion flux to the divertor plate.

The simple two-point model of the divertor [62] gives the following scalings for the divertor parameters as a function of the separatrix temperature (or the power flow into the SOL) and the separatrix density :

$$n_d = \left(\frac{7 \quad \gamma \quad L_c}{8 \quad \kappa_0 \quad \sqrt{m_i}} \right)^2 \frac{n_s^3}{T_s^4} \tag{1}$$

$$T_d = \frac{1}{2} \left(\frac{8 \quad \kappa_0 \quad \sqrt{m_i}}{7 \quad \gamma \quad L_c} \right)^2 \frac{T_s^5}{n_s^2} \tag{2}$$

$$T_s = \left(\frac{7 \quad L_c^2}{4\kappa_0 \quad 2\pi R \quad 2\pi a \quad \Delta} \right)^{2/7} (P_{sol})^{2/7} \tag{3}$$

where n_s, T_s are the density and temperature at the separatrix, n_d, T_d are the density and temperature at the divertor, P_{SOL} is the power flux from the main plasma into the SOL, γ is the sheath transmission coefficient, κ_0 is the electron thermal conductivity coefficient, m_i is the ion mass, R is the major radius of the tokamak, a is the minor radius, L_c is the connection length from the stagnation point (or watershed) to the divertor target in the SOL and Δ is the SOL width. In the above derivation it has been assumed that there are no significant energy and momentum losses in the SOL, there is no pressure loss along the field lines and that the electron and ion temperature are the same.

Within these approximations the divertor ion flux is given by :

$$I_d = n_d c_d = \left(\frac{7 \quad \gamma \quad L}{8 \quad \kappa_0 \quad m} \right) \frac{n_s^2}{T_s^{3/2}}. \tag{4}$$

Hence, the ion flux scales with the square of the separatrix SOL density under the above approximations. We use this scaling as a reference to quantify the degree of detachment achieved in the experiment.

In order to apply this scaling to the experimental data, we start by selecting a series of discharges (or a single density ramp discharge) with the same input power. We then take the

measured ion flux at the divertor for low density conditions and extrapolate its value for higher densities assuming a square law dependence on the main plasma density (which is assumed to be proportional to the separatrix density). In this way, we obtain the extrapolated ion flux following the two point model :

$$I_d^{scal} = C \quad \left\langle \overline{n_e} \right\rangle^2 \tag{5}$$

where I^{scal}_{d} is the extrapolated "attached" divertor ion flux, $\langle n_e \rangle$ is the main plasma line average density and C is a normalisation constant, which is obtained experimentally from the low density phase of every density ramped discharge (or series of discharges) considered. We use this procedure not only for the separatrix ion flux but also for the integrated ion flux to the divertor and the maximum ion flux to the divertor. A comparison of the extrapolated ion flux and the measured ion flux, obtained using the above procedure, is shown in Fig. 45, for the inner and outer divertor of an Ohmic density ramp. The same normalised scaling is used for the separatrix ion flux, the integral ion flux and the peak ion flux (which may be found in different flux tubes, at different stages of the discharge) for both the inner and outer divertor. One may notice from Fig. 45 that while the integrated ion flux to the outer divertor follows the two-point model scaling up to the onset of detachment, the peak and separatrix ion flux increase more rapidly. This effect is due to the strong peaking of the divertor ion flux profiles highlighted towards the end of section 3.1.3.

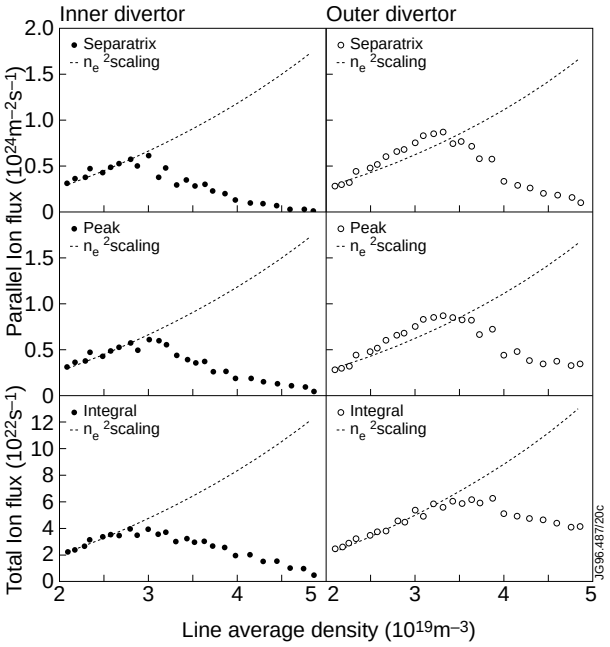

Fig.45: Measured and extrapolated ion flux to the inner and outer divertor for an Ohmic density ramp. The same quadratic law is used for the separatrix ion flux, the peak ion flux to the divertor and the integral ion flux both to the inner and the outer divertors.

Based on this very simple scaling, which is adequate for our purposes, we define the degree of detachment (D.O.D.) as the ratio of the extrapolated ion flux (following Eq. 5) to the measured ion flux (separatrix, peak or integral) as follows:

$$\text{D.O.D.} = \frac{I_d^{scal}}{I_d^{measured}} \tag{6}$$

When the experimental scaling with density is stronger than quadratic, this definition gives values smaller than one, indicating that the flux amplification is higher than that expected from simple models. Detachment can be identified as the point at which the degree of detachment starts to be significantly larger than unity.

This new method of characterising detachment produces very similar results to the typical procedure based upon the measured parallel pressure drop between the SOL and the divertor which is associated with divertor detachment [63,64,9]. It has the advantage, however, that divertor ion flux measurements are generally more readily avaliable that the pressure and do not rely upon accurate determination of the SOL seperatrix location. In fact, the degree of detachment is very closely linked to the pressure drop along the field from the SOL to the divertor since one can show that :

$$\text{D.O.D.} = \frac{n_d^{scal}\ c_d^{scal}}{n_d^{measured}\ c_d^{measured}} = \frac{n_s^{scal}\ T_s^{scal}}{2\ n_d^{measured}\ T_d^{measured}} \sqrt{\frac{T_d^{measured}}{T_d^{scal}}} \tag{7}$$

Hence, provided that the two point model extrapolated values are similar to those of the experiment, the degree of detachment and the pressure drop from the SOL to the divertor have a very similar magnitude. Despite the simplicity of the models used here to define the D.O.D., the comparison between the pressure drop and the D.O.D. is remarkably good (see Fig. 46) and justifies the use of the degree of detachment as standard tool to characterise this regime in divertor discharges.

The definition of the degree of detachment is, however very simple, and has to be modified appropriately, if it is used to characterise more complicated divertor detachment scenarios such as those which involve impurity seeding [11]. Using similar assumptions than those for Eqs. 1-4, but including now the proportion of radiated power

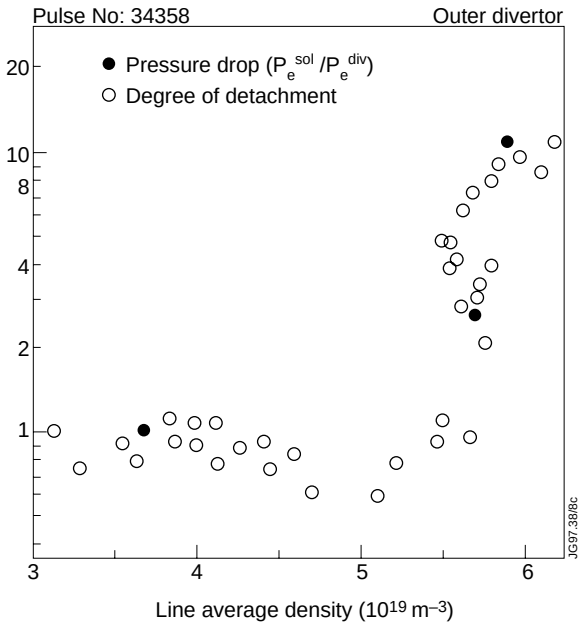

Fig.46: Measured outer divertor peak pressure drop (filled circles) for an L-mode density ramp discharge (that of Fig. 18) compared with the derived degree of detachment (open circles) showing remarkably good agreement between both definitions used to characterise divertor detachment.

in the SOL ($\Re$) that is derived approximately from the experimental bolometer measurements, it can be shown that the appropriate reference scaling for the divertor ion flux under those conditions is modified as follows:

$$I_d^{scal} = C \quad \frac{\langle n_e \rangle^2}{1 - \Re}. \tag{8}$$

We shall use this definition when discussing the degree of detachment for impurity seeded H-modes.

By separately carrying out the D.O.D. estimate for the ion flux integral, ion flux at the separatrix and the peak ion flux, it is possible to distinguish between the onset of detachment for various configurations and the differences between partial detachment and total detachment. One such example for which the degree of detachment has been calculated is shown in Fig. 47 using the scaling shown in Fig. 45. During the onset partial detachment, the separatrix ion flux is seen to drop in the experiment and, correspondingly, the degree of detachment starts to increase from the attached value (close to unity). However, at this stage, the integral ion flux does not decrease significantly and as a result the degree of detachment stays close to unity for the ion flux integral. At the onset of total detachment, the degree of detachment for all three measurements (separatrix, peak and integral) increase considerably (typically more than an order of magnitude). Following these comments, it can be clearly seen from Fig. 47 that only partial detachment is achieved at the outer divertor before the density limit disruption and the separatrix degree of detachment reaches 13, while the integral degree of detachment only reaches 3. In contrast, the inner divertor exhibits total detachment since the separatrix degree of detachment reaches 90 and the integral degree of detachment reaches 22.

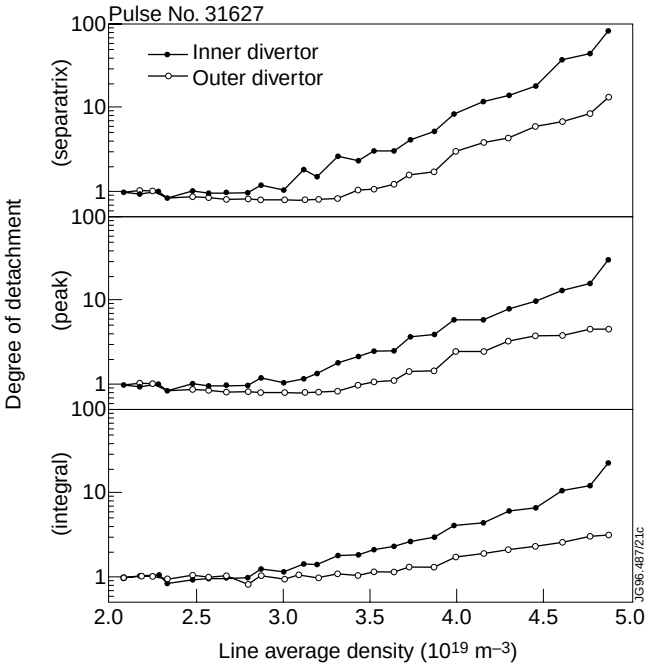

Fig.47: Measured degree of detachment for the discharge of Fig. 45 for the separatrix, peak, an integral ion flux for both the inner and the outer divertors, versus line average density. Note the large degree of detachment reached at the inner divertor typical of total divertor detachment.

Given that detachment is a gradual process, it is difficult to define precise borders that distinguish weakly detached plasmas from attached plasmas. For JET discharges we have found that a convenient set of criteria to characterise detachment in most regimes is shown in the following table :

Detachment state	D.O.D.^{peak}	D.O.D.^{integral}
Partial Detachment	>2	<10
Total Detachment	>2	>10

Consequently, the window of divertor detachment may be defined as the density range between the onset of divertor detachment (D.O.D.^{peak} > 2) and the density limit for either divertor . The density limit in this context is given by the formation of a MARFE in the main plasma for Ohmic and L-mode discharges or the loss of confinement in H-modes.

Using the D.O.D. definition we can compare, in a quantitative way, the influence of the factors considered in previous sections of the paper on divertor detachment. In Fig. 48 we examine the dependence of the degree of detachment (separatrix, peak and integral) on magnetic configuration for a series of Ohmic density ramps with forward toroidal field. Although there is some scatter for discharges with the same magnetic configurations (probably due to different machine conditions), it is clear that the degree of detachment reached before the density limit is similar in all configurations. However, clear dependencies are highlighted, which we have already discussed, such as the lower density at which high flux expansion discharges detach and their smaller detachment window. For the reasons explained in section 4.1.1, it is meaningless to calculate the integral degree of the detachment for vertical plate divertors, as it depends on the precise strike point position, which changes continuously with strike point sweeping. Hence, we can only compare the degree of detachment for the separatrix and the peak ion flux when the separatrix is located at the lower part of the vertical plate. It is worth noting that the window of stable detachment is similar for both vertical and low flux expansion horizontal divertors. Fig. 48 also shows a more symmetric (inner/outer divertor) detachment for vertical divertor discharges. It is also clear that for the horizontal divertor discharges it is only possible to achieve, in a stable way, discharges in which the outer divertor is partially detached (integral degree of detachment around 4) while the inner divertor is totally detached (integral degree of detachment around 20).

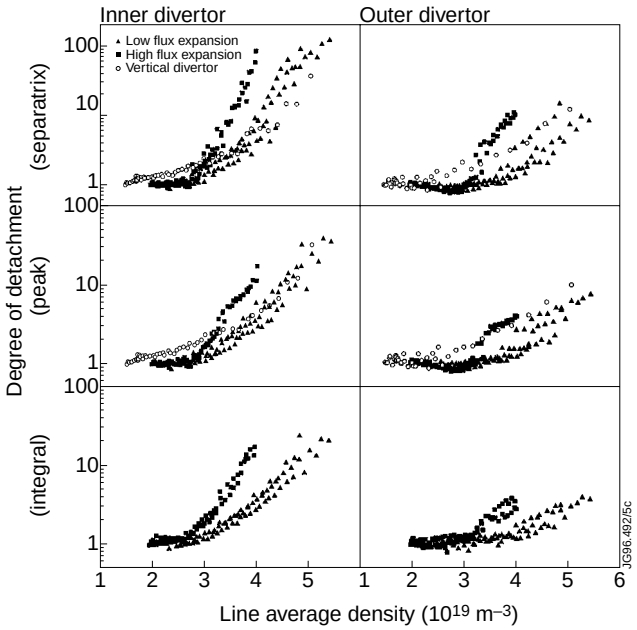

Fig.48: Measured degree of detachment (separatrix, peak and integral ion flux for both the inner and the outer divertors) for a series of Ohmic discharges with different magnetic configurations, versus line average density.

In Fig. 49, we compare the dependence on magnetic configuration of the degree of detachment (peak and integral) for a series of L-mode density ramps with forward toroidal field. For this regime, there is more scatter in the plots (particularly for the peak value) because of the appearance of divertor oscillations (section 3.2) with the onset of detachment. The first difference to be noticed in these plots, with respect to those of the preceding figure, is the higher densities that are achieved. This is associated with a weak dependence of the detachment density and density limit on the input power (also illustrated below). For L-mode discharges, the detachment window does not depend strongly of the magnetic configuration, with differences of approximately 10-15 % in the maximum density achieved in different configurations. One striking difference in the onset of detachment for L-mode discharges compared to Ohmic ones, is the strong dependence of the degree of detachment on the plasma density. This steep rise of the degree of detachment with main plasma density coincides with the decay of the divertor oscillation. It is also worth noting that the maximum integral degree of detachment that can be achieved in a stable manner for L-mode is a factor of 2-3 larger than that achieved in similar Ohmic discharges.

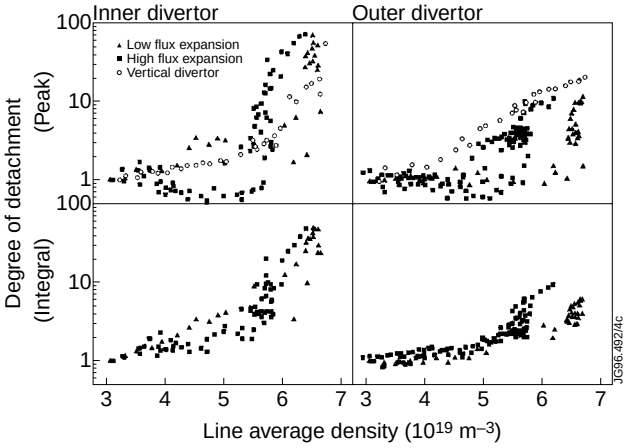

Fig.49: Measured degree of detachment (separatrix, peak and integral ion flux for both the inner and the outer divertors) for a series of L-mode discharges (4MW of neutral beam heating) with different magnetic configurations, versus line average density. The increased scatter in the data is due to the presence of divertor oscillations.

While the previous figures used to illustrate the degree of detachment are plotted versus line average density, the physical parameter that controls the detachment process is the electron temperature in the divertor region. The differences seen in the plots versus density are only associated with the differences in the divertor electron temperature for each configuration. This is illustrated in Fig. 50, where we have re-plotted the degree of separatrix detachment at the outer divertor for a series of Ohmic density ramps on the horizontal divertor with high and low flux expansion (those of Fig. 48) versus the separatrix electron temperature at the divertor as measured by Langmuir probes. It is clear that the differences between high and low flux expansion illustrated in Fig. 48 disappear when the temperature is assumed to be the key controlling parameter that characterises divertor detachment. However, it is more convenient to use the main plasma line average density as the independent variable since this is the parameter that is controlled in the experiment and we will continue to use it throughout this section. Nevertheless, it must be stressed that the physical parameter that controls detachment is the divertor electron temperature.

The degree of detachment can also be used to illustrate quantitatively the strong dependence of detachment on the strike point position on the vertical plate. This is shown in Fig. 51, where

we have plotted the measured degree of detachment for three probes located at different heights on the vertical plate, for L-mode density ramp discharges with forward field. When the separatrix is located at the lower part of the vertical plate, it is possible to achieve a similar degree of detachment to that on the horizontal plate. However, when the separatrix is located at the upper part of the vertical plate the discharges remain more attached up to the onset of the density limit disruption.

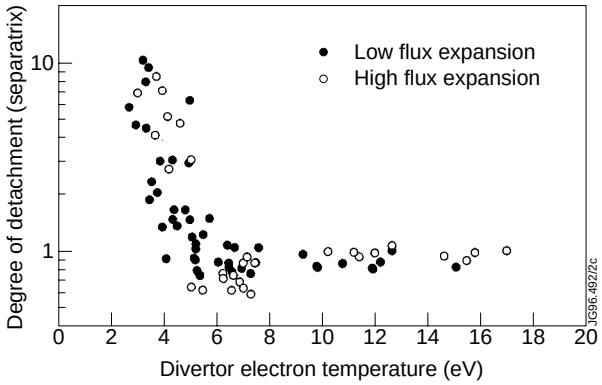

Fig.50: Measured degree of separatrix detachment versus separatrix electron temperature at the divertor for the horizontal plate discharges shown in Fig. 48.

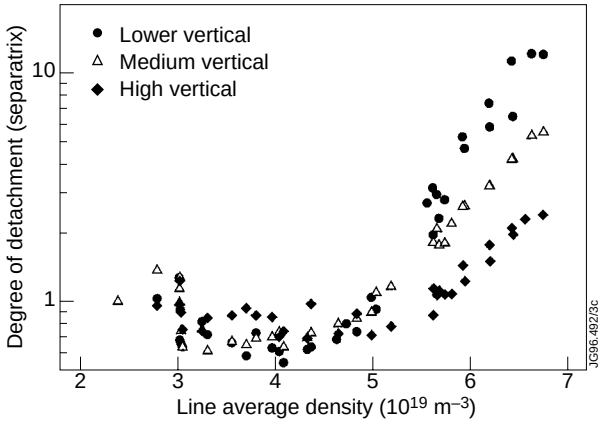

Fig.51: Measured degree of separatrix detachment versus line average density for probes at different positions at the vertical target during L-mode density ramp discharges. Note the reduced degree of detachment reached at the upper part of the vertical plate.

From Figs. 48 and 49, it is obvious that the density at which detachment is observed and the maximum density achieved increase weakly with the input power. In order to study this behaviour while minimising the uncertainty associated with varying machine conditions, an experiment was performed in which the detached divertor regime was explored for Ohmic, L-mode and H-mode conditions in a series of consecutive discharges. The results of this experiment are shown in Fig. 52 for the peak and integral degree of detachment at the inner and the outer divertor. The discharges with additional heating achieve higher densities in a stable way, particularly in the case of the L-mode. However, the reader is reminded that the characteristics of detachment in Ohmic and L-mode, as compared to those in H-mode, are

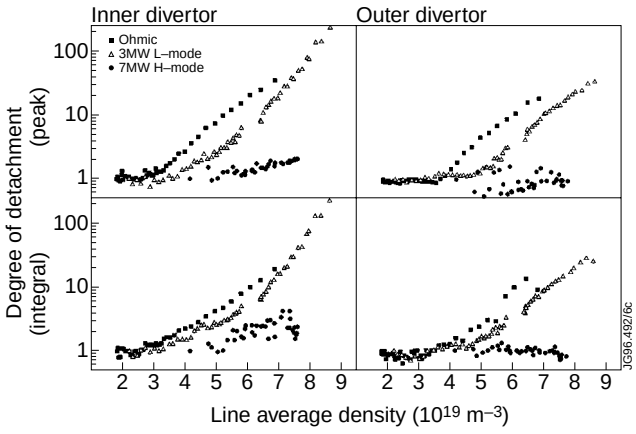

Fig.52: Measured degree of detachment versus line average density at several levels of input power (Ohmic, L-mode 3.5 MW and H-mode 7 MW). Note the larger densities achieved with higher input power and the lower degree of detachment for the same density, with increasing input power. The scatter in the H-mode points is due to ELMs.

very different. Whereas for Ohmic and L-mode regimes the density range is controlled by the density limit disruption, the density range in H-mode is limited by the degradation of confinement that occurs at high gas fuelling rates. From Fig. 52 one can also see that this difference is evident from the degree of detachment reached by the Ohmic and L-mode discharge, as compared to the H-mode, which barely detaches at the inner divertor before the H-mode confinement is lost (note that the scatter in the H-mode experiments is due to the presence of ELMs). Hence, we have demonstrated that the window of divertor detachment is weakly expanded with additional heating while the discharge remains in the L-mode. Unfortunately, this expansion of the operating window cannot be fully exploited to achieve high densities because, as the input power is increased, the discharge undergoes a transition into H-mode confinement after which the plasma density is primarily determined by the particle confinement associated with this regime of confinement rather than external gas fuelling.

As discussed in section 3.3, with deuterium fuelling in H-mode discharges it is possible to detach in-between the ELM events. This is clearly illustrated in Fig. 53 for a 10MW density ramp H-mode where the degree of detachment is plotted at the inner and outer divertor for the ion flux (a) during ELMs, (b) between ELMs and (c) integrated. One can clearly see that a large D.O.D. can be obtained in-between the ELM events (particularly at the inner divertor) but that the integral is reduced by significantly less. During the ELM events there is no preferential reduction in the ion flux at the inner divertor and this is because the reduction in ELM amplitude is mainly associated with the increased ELM frequency rather than detachment. It is important to highlight that the loss of confinement observed in high density H-modes is correlated to the detachment of the divertor. This is illustrated in Fig. 54 where the confinement is shown to deteriorate as detachment progresses. Ultimately, this loss of confinement dictates the maximum attainable density in H-mode to values typically below that of the Greenwald limit [48] as shown in Fig. 55. The confinement

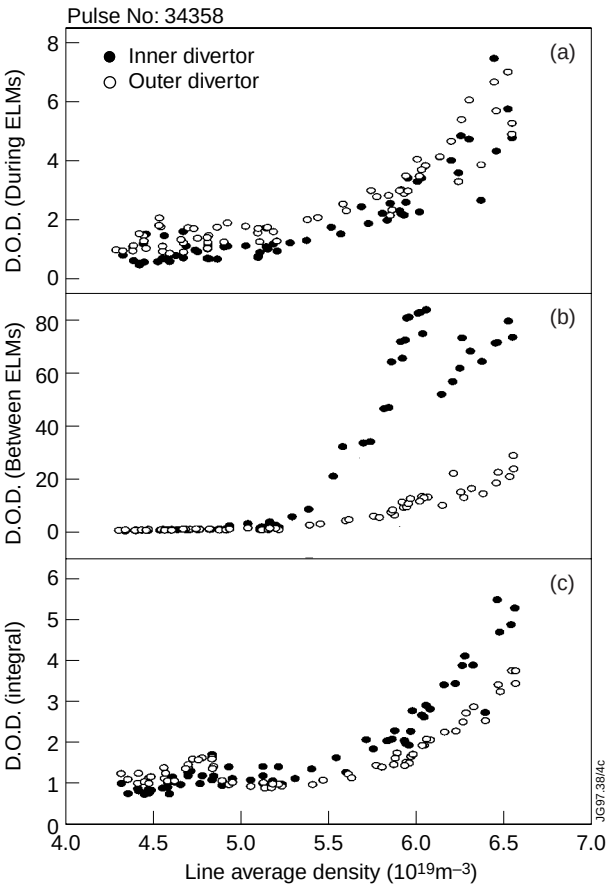

Fig.53: Measured peak degree of detachment during ELMs (a) and between ELMs (b) for an H-mode density scan (11 MW of NBI). Note the low degree of detachment reached at the ELMs for both divertors with the large degree of detachment reached at the inner divertor between the ELMs. This is characteristic of detachment in H-modes where the divertor is detached between ELMs and reattaches at the ELMs. The integral degree of detachment (c) includes the ELMs in its calculation and remains under 10 up to the highest densities.

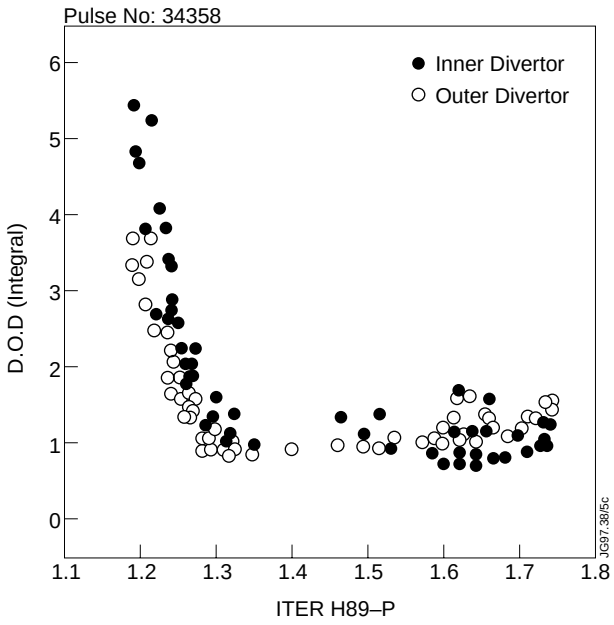

Fig.54: Measured integral degree of detachment versus energy confinement (normalised to the ITER-89P L-mode scaling) for the H-mode density scan of Fig. 53. As detachment proceeds the energy confinement deteriorates reaching values close to L-mode at the highest detachment.

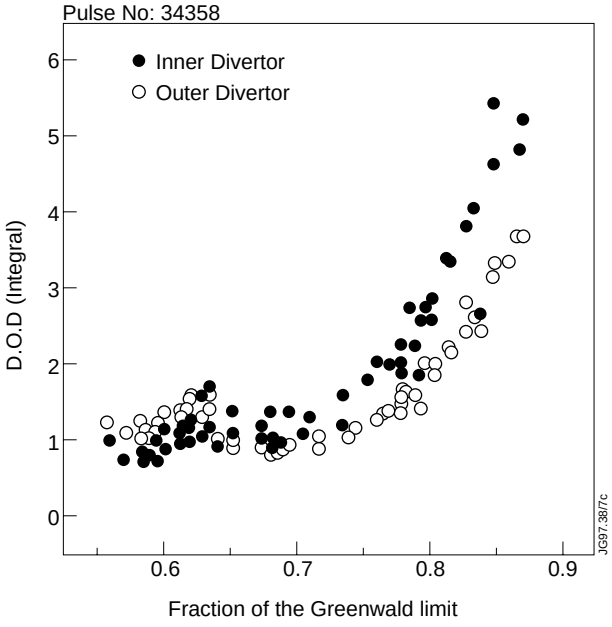

Fig.55: Measured integral degree of detachment versus plasma density (normalised to the Greenwald value) for the H-mode density scan of Fig. 53. As the density approaches the Greenwald value the degree of detachment increases and confinement deteriorates (see Fig.54).

loss may be due to the increase of neutral pressure in the main chamber (Fig. 56) which has been previously shown to adversely affect H-mode performance [16,46]. However, at present it is difficult to determine the causality of the confinement loss and it is also possible that the perturbation to edge gradients caused by the MARFE moving to the x-point region could be the dominant effect.

Similarly, have used the degree of detachment definition to illustrate the benefit in terms of detachment of several impurity seeded H-modes compared to the corresponding deuterium gas puffed discharges. In Fig. 57 we have plotted the degree of detachment achieved versus confinement time (normalised to the ITER H-89P scaling) for a series of H-mode discharges (cryopump on) where several impurity species

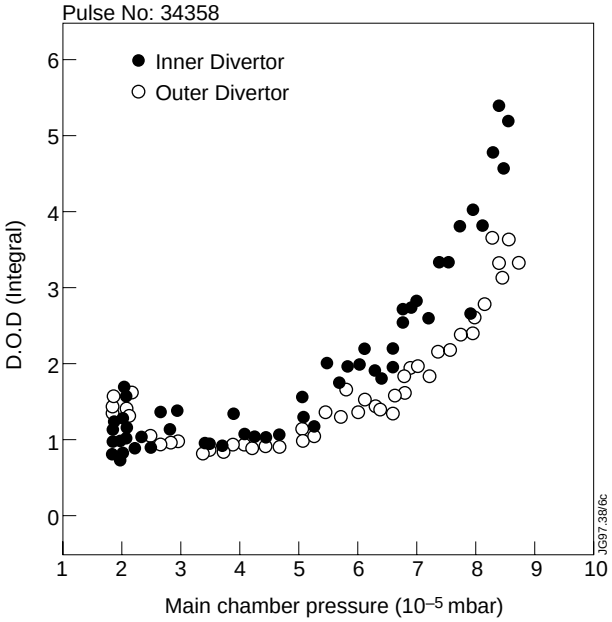

Fig.56: Measured integral degree of detachment versus main chamber neutral pressure for the H-mode density scan of Fig. 53. With increasing degree of detachment the neutral pressure in the main chamber increases. Figs. 53-56 show the interdependence of detachment, energy confinement, main chamber neutral pressure and density limit in H-mode discharges. While it is obvious that all four factors are linked, is not clear, at present, which is the one that drives the observed phenomena.

have been injected. It is clear that puffing Nitrogen leads to a larger degree of detachment while maintaining a better confinement than discharges in which only deuterium is puffed, although at the expense of an increased impurity content in the main plasma. Neon seeding does not have any major advantage with respect to Deuterium puffing or Nitrogen which is probably due to the fact that it radiates more in the main plasma than Carbon and Nitrogen which leads to a large confinement deterioration before detachment can be achieved.

The dependence of detachment on toroidal field direction is shown in Fig. 58 for the peak degree of detachment, at the inner and outer divertor, for Ohmic discharges at the horizontal divertor with low flux expansion and corner configuration. The onset of detachment occurs at similar densities for either direction of the toroidal field while the symmetry of the detachment changes not only with field

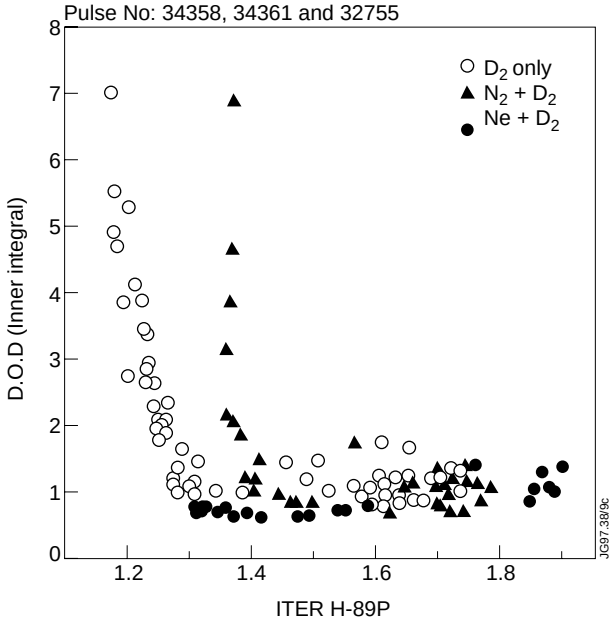

Fig.57: Inner divertor integral degree of detachment for a series of H-mode discharges (11MW of NBI) with deuterium puffing alone and with Neon and Nitogen seeding versus energy confinement (normalised to the ITER-98P scaling). Note the larger degree of detachment achieved for discharges with Nitrogen seeding, while maintaining an improved confinement. This behaviour is not observed with Neon seeding which is probably related to the temperature dependence of its radiation efficiency.

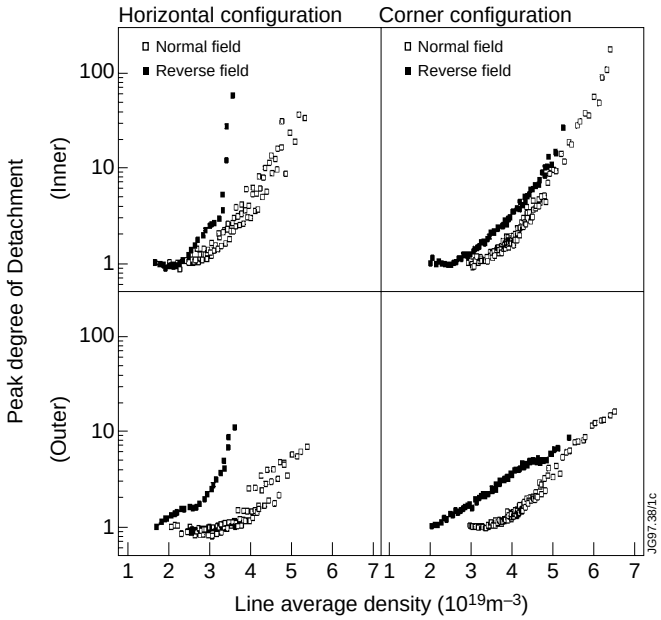

Fig.58: Measured degree of peak detachment versus line average density for Ohmic discharges on the horizontal divertor (low flux expansion) and corner configuration with forward and reversed field.

direction but also with magnetic configuration. While for low flux expansion horizontal divertor detachment is more symmetric for reversed field discharges, for the corner configuration the forward field discharges reach detachment more symmetrically. In any event, the reversed field discharges do not have a broader detachment window, as had been previously anticipated, since they reach the density limit at similar (or somewhat lower) main plasma densities than forward field discharges under the same plasma conditions.

In vertical plate L-mode discharges with reversed field the outer divertor is very resistant to detachment. This makes the final state reached by the plasma more asymmetric for reversed field vertical plate L-modes, than comparable discharges with forward field. Fig. 59 shows the degree of peak detachment for L-mode discharges with the strike zone at the lower part of the target and with forward and reversed field. The range of stable operation is similar for both directions of the field but the degree of detachment reached, in particular at the outer divertor, is much smaller than for discharges with reversed field. For this reason, the experiments with the reversed toroidal field were not pursued further, as they do not provide any benefit with respect to the achievement of detachment compared to those with forward field and have a significantly higher H-mode threshold.

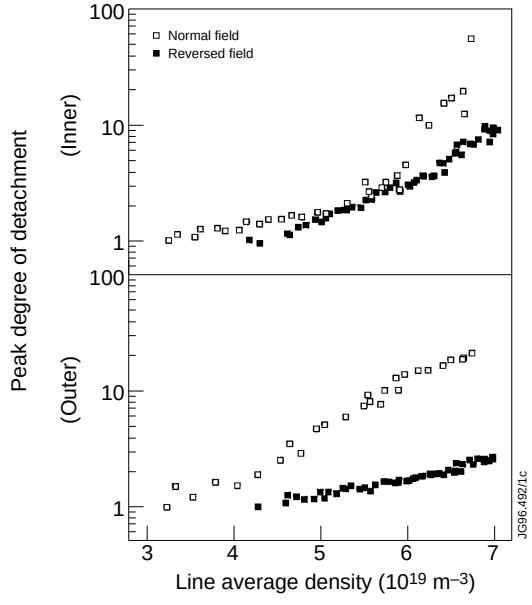

Fig.59: Measured degree of peak detachment versus line average density for L-mode discharges on the vertical target and forward and reversed field. The range of densities achieved in a stable way is similar for both directions of the field but the degree of detachment obtained at the outer divertor is much smaller for reversed field discharges.

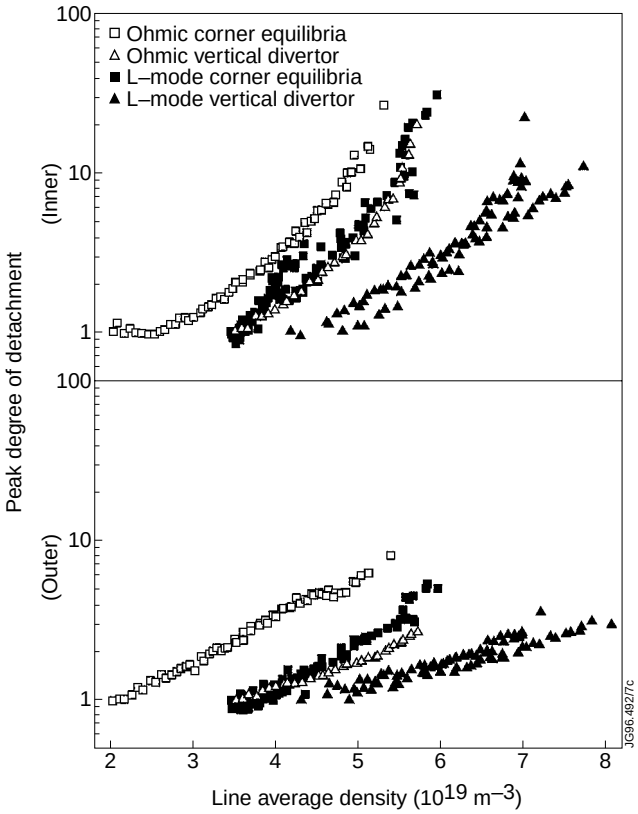

Fig.60: Measured degree of peak detachment versus line average density for Ohmic and L-mode discharges with reversed field and several divertor configurations. The detachment window is widened with the additional power (particularly for vertical plate discharges). However, the degree of detachment obtained at the outer divertor is very small for L-mode discharges.

The effect of configuration on detachment has also been explored for discharges with reversed toroidal field in Ohmic and L-mode regimes Fig. 60. The increase of the detachment window with additional heating is also found for discharges with reversed field and it is particularly large for vertical plate divertor discharges. However, it is also important to note that the degree of detachment achieved for the peak ion flux is very small in this case, particularly for the outer divertor, which shows again the problem of the unstable approach to detachment for reversed field discharges already discussed above.

7. CONCLUSIONS

In this paper we have presented results from dedicated experiments carried out to characterise plasma detachment in the JET Mark I divertor. New and enhanced diagnostic systems have provided detailed measurements of core, scrape-off layer (SOL) and divertor plasma parameters on the approach to detachment. Experiments have been carried out to assess the range over which divertor detachment is observed in Ohmic, L-Mode and ELMy H-mode confinement regimes. In addition, the effect of additional parameters has been considered including, the divertor configuration, direction of the toroidal field, divertor target material and the influence of active pumping. Finally, the concept of the "degree of detachment" has been introduced as a quantitative means of comparing the results from the whole range of experiments described above.

During Ohmic discharges in which the density is increased by gas fuelling, it is observed that the divertor exhibits the three characteristic phases of low recycling, high recycling and detachment. The low recycling phase is shown to be characterised by small parallel temperature and density gradients which increase as the high recycling regime is accessed. The ratio of the total ion flux to the total D_α emission from the divertor is approximately 20 and in good agreement with the calculated Johnson-Hinnov factor. As the divertor electron temperature approaches 5eV, firstly at the inner divertor, the ion flux "rolls-over" and begins to decrease, indicating the onset of detachment. During this phase it is observed that the parallel electron pressure is no longer conserved in the SOL. Throughout the transition from low to high recycling and detachment, it is shown that the SOL broadens considerably, highlighting the importance of providing sufficient clearance between the separatrix and vessel walls. The degree and spatial extent of the detachment reached in the experiment (as determined from the divertor ion flux profiles) show that the inner divertor is completely detached while the outer is only partially detached. These measurements have also allowed enhanced perpendicular transport to be eliminated as the mechanism which accounts for the reduction in parallel ion flux during detachment. While the divertor ion flux is observed to decrease during detachment, the divertor D_α emission and subdivertor neutral pressure continue to increase. In principle, these seemingly contradictory observations can be partially reconciled with the model proposed by Stangeby [29] in which the plasma momentum is removed by charge-exchange collisions with recycling neutrals. It is also shown that the decrease in the number of ionisations per D_α photon at the

outer divertor may be explained by the change in the Johnson-Hinnov factor resulting from the decrease in divertor electron temperature and density during detachment. However, the order of magnitude decrease in the total ion flux at the inner divertor cannot be reconciled in this way and additional processes such as volume recombination must be invoked. Experimental evidence is presented for changes in the D_γ/D_α ratio that are consistent with volume recombination processes taking place. During the final stages of detachment, the ionisation front and peak radiation emission are observed to migrate away from the target to the X-point region.

Similar general trends for detachment are observed during density ramp experiments in L-Mode neutral beam heated (NBI) discharges. During these discharges, the onset of detachment and the density limit occur at higher main plasma density than comparable Ohmic cases. Unfortunately, this trend is weaker than simple scalings based upon $\sqrt{P_{INPUT}}$, since the divertor radiative losses increase with input power. The total radiation level at which detachment begins in Ohmic and L-mode discharges is typically 50-60%, of which around 50% of the power entering the SOL is radiated in the divertor region. Stable detachment can be obtained in L-mode discharges and feedback control of the gas fuelling using the divertor ion flux measurements has been successfully demonstrated. One distinctive feature of L-mode discharges is the occurrence of the so-called divertor oscillations, which are observed as large amplitude variations in the divertor ion flux during the approach to detachment. This complicated phenomenon also affects the temperature and density profiles in the outer region of the core plasma and it is proposed that impurity production at the divertor target coupled with the instability of the MARFE position controls the oscillations.

Due to the presence of ELMs, the general character of H-mode discharges is different from the Ohmic and L-Mode cases. As the gas fuelling is increased in H-mode discharges, the ELMs decrease in amplitude and increase in frequency. Beyond certain levels of gas fuelling, the confinement deteriorates and this ultimately limits the maximum density and radiated power fraction (50%) that can be attained in H-mode. Nevertheless, similar detachment behaviour of the ion flux and D_α emission is observed, albeit between ELM events. During the ELM event, detachment is not sustained and large ion fluxes are measured at the divertor target, although the divertor D_α emission may actually decrease. These so-called “negative” ELMs may be understood by taking into account changes of the Johnson-Hinnov factor resulting from the energy pulse associated with the ELM.

Detailed experiments have been carried out to assess the influence of divertor geometry and wall clearance on plasma detachment. It is shown that Ohmic discharges with low wall clearance have lower threshold densities for detachment and density limit by about 35%. This results can be related to the relative proportions of bulk and divertor plasma radiation, the fraction of bulk radiation being significantly higher in the low wall clearance discharges. Experiments to assess the effect of divertor flux expansion for discharges with the strike zones on the horizontal targets are complicated by the wall clearance issue. In the case of the high flux expansion

configuration, the wall clearance is reduced and this lowers both the threshold density for detachment and the density limit by the same degree as is observed for experiments in which the wall clearance is reduced independently of the flux expansion. These observations lead to the conclusion that the wall clearance may be the dominant effect in these experiments rather than the flux expansion. Similar behaviour is observed during L-mode discharges although the influence of wall clearance was found to be much weaker.

In the JET Mark I divertor configuration, it is possible to operate with the strike zones located on either the horizontal or vertical target plates and experiments have been carried out to assess the relative merits of these configurations. In contrast to predictions from 2D modelling codes, there were no significant differences between the onset of detachment and the density limit for the two configurations. Detailed comparisons of the ion flux profiles for the vertical target case show that the detachment occurs over a smaller density range for the inner and outer divertor and that the degree of detachment is larger at the lower part of the vertical plate. It should, however, be stressed that the degree of detachment on any part of the vertical plate is never larger than for the horizontal target. There is some evidence that the presence of neutral by-pass leaks and the existence of an inwards SOL particle pinch may yet account for the discrepancies between code and experiment.

Dedicated experiments have been carried out to assess the effect of the toroidal field direction on the detachment behaviour in JET. It was expected that, due to the more symmetric divertor plasma parameters in reversed field discharges, the onset of detachment should occur over a smaller density range for the inner and outer divertors. This has been only confirmed for one divertor configuration while it seems to produce the opposite effect in the rest of configurations. Regardless of divertor configuration, almost immediately after detachment, the reverse field discharges form a MARFE in the main plasma, which produces a density limit. The levels of radiated power are similar for both forward and reversed field, so that this behaviour cannot be explained by increased impurity contamination. In the case of L-mode reversed field discharges, it was also not possible to obtain steady-state detached plasmas.

By using the cryopump installed in the JET Mark I divertor, the influence of active pumping on detached plasmas has been studied. It was found that the overall density threshold for detachment and the density limit are similar with and without active pumping. However, during some Ohmic discharges the inner divertor is observed to re-attach when moved into the corner region of the divertor where the maximum particle removal rate is obtained, thereby highlighting the importance of large divertor neutral pressures to achieve detachment.

An important aspect of the JET Mark I divertor campaign was to assess the relative merits of Carbon and Beryllium as divertor target materials. In terms of the approach to detachment, the general behaviour of discharges with different divertor target materials is very similar. It should, however, be highlighted that throughout this comparison, the other first wall components were unchanged and, as a result, Carbon remained the dominant impurity species. Clear differences

in the sputtering behaviour of the divertor are observed between Carbon and Beryllium targets on the approach to detachment associated with the absence of chemical sputtering for Beryllium. It is also found that the ratio of Carbon to Hydrogen radiation is highest for discharges with low wall clearance. However, contrary to expectations the impurity contamination of the core plasma does not increase on the approach to detachment, even when the region of peak radiation is located at, or above, the X-point region. Such observations indicate that the impurities may be well confined within the MARFE, or that the impurity contamination does not depend strongly on the divertor regime.

In order to compare and contrast all the results described above it is convenient to develop a quantitative scaling by which the "degree of detachment" may be defined in terms of the main plasma density. We use the result from the two-point model for the quadratic dependence of the divertor ion flux on main plasma density and compare it with the measured ion flux from low to high recycling and then extrapolate it through to detachment. The degree of detachment is then defined as the ratio of the extrapolated ion flux to the measured ion flux.

Such an analysis has been carried out using the JET discharges described in this paper for the separatrix, peak and integrated ion flux at both the inner and outer divertors. The results presented earlier in the paper are subsequently reinforced by this definition, which conveniently highlights the distinctions between complete and partial detachment among other effects. This quantitative definition of detachment leads to the introduction of the detachment window for both divertors as the density range over which either divertor is detached (D.O.D.^{peak} > 2) up to the density limit. The detachment window diagrams can be used to summarise the experimental observations of plasma detachment and compare its dependency on the parameters controlled in the experiment. Two examples of such diagrams are shown in Fig. 61 and Fig. 62 which display some of the dependencies of divertor detachment found in JET Mark I divertor experiments with magnetic configuration, level of additional heating, and toroidal field direction.

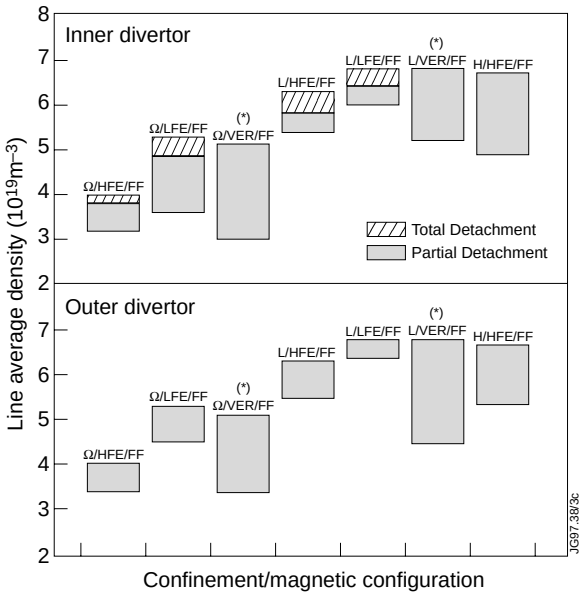

Fig.61: Detachment window for the inner and outer divertor for various divertor magnetic configurations (HFE = High Flux Expansion, LFE = Low Flux Expansion, VER = Vertical Divertor) and confinement regimes (Ω, L and H-mode) with forward direction of the toroidal field. Due to the effect of strike point sweeping on vertical divertor discharges we have only indicated the window over which there is plasma detachment on the lower part of the vertical plate as indicated by the asterisk.

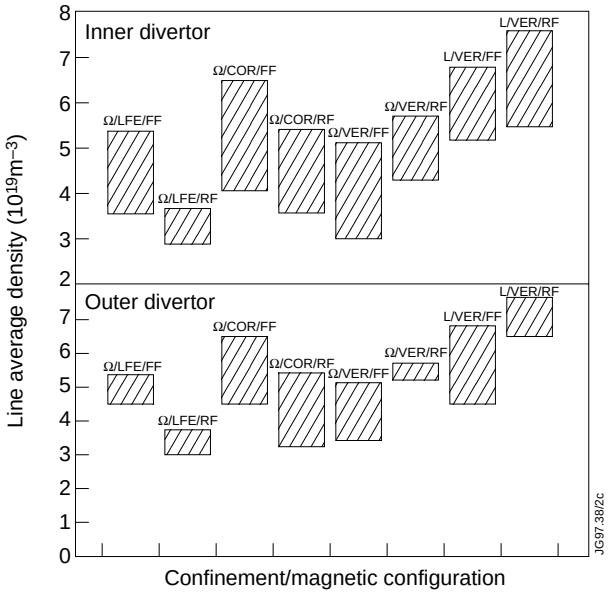

Fig.62: Detachment window for the inner and outer divertor for various divertor magnetic configurations (HFE = High Flux Expansion, LFE = Low Flux Expansion, VER = Vertical Divertor) and confinement regimes (Ω, L) with forward and reversed field.

Finally, we propose the quantitative framework offered by the definition for the "degree of detachment" as the tool to compare experiments from different divertor tokamaks.

ACKNOWLEDGEMENTS.

It is a pleasure to acknowledge the contributions from many members of the JET Divertor Task Force and the JET Team to this paper. We are particularly grateful to P.C. Stangeby, K. Borrass, A. Taroni, R. Simonini, J. de Haas, P.D. Morgan, Y. Ul'Haq, A. Rookes, L. Porte and A. Tabasso for contributing experimental data and/or fruitful discussions. One of the authors (A.L.) wishes to acknowledge helpful discussions with members of other divertor tokamak experiments and ITER Divertor Experts groups.

REFERENCES

[1] P.H Rebut, D. Boucher, D.J. Gambier, et al., Fusion Eng. and Design **22** (1993) 7.

[2] G. Janeschitz, K. Borrass, G. Federici, et al., J. Nucl. Mater. **220-222** (1995) 73.

[3] M. L. Watkins and P. H. Rebut, Controlled Fusion and Plasma Physics (Proc. 19th Eur. Conf. Innsbruck, Austria, 1992), vol. 16C, part II, p.731.

[4] K. Borrass, G. Janeschitz, Nucl. Fusion **34** (1994) 1203.

[5] S. Clement, S.K. Erents, N. Gottardi, et al., 33th Conf. Am. Phys. Soc. Plasma Phys. Div., Tampa, USA, 1991, JET Report JET-IR(91)11.

[6] T. Petrie, D. Buchenauer, D. Hill, et al., J. Nucl. Mater. **196-198** (1992) 848.

[7] G. Janeschitz, S. Clement, N. Gottardi, et al., Controlled Fusion and Plasma Physics (Proc. 19th Eur. Conf. Innsbruck, Austria, 1992), vol. 16C, part II, p.727.
[8] M. Laux, K. Buechl, A. Carlson, et al., Controlled Fusion and Plasma Physics (Proc. 20th Eur. Conf. Lisboa, Portugal, 1993), vol. 17C.
[9] B. Lipschultz, J. Goetz, B. LaBombard et al., J. Nucl. Mater. **220-222** (1995) 50..
[10] L.D. Horton and the JET Team, Plasma Phys. & Control. Nucl. Fus. Res. (Proc. 15th Int. Conf. Plasm. Phys. & Control. Fus. Res.) vol.1 (1995) 541.
[11] G.F. Matthews and the JET Team, Plasma Phys. & Control. Fusion **37A** (1995) A227.
[12] N. Hosogane, K. Itami, N.Asakura, et al., J. Nucl. Mater. **220-222** (1995) 420.
[13] D.J. Campbell and the JET Team, Plasma Phys. & Control. Nucl. Fus. Res. (Proc. 15th Int. Conf. Plasm. Phys. & Control. Fus. Res.) vol.1 (1995) 527.
[14] M. Keilhacker and the JET Team, Plasma Phys. & Control. Fusion **37A** (1995) A3.
[15] R. Satori, S. Ali-Arshad, E. Bertolini et al., Controlled Fusion and Plasma Physics (Proc. 22th Eur. Conf. Bournemouth, United Kingdom, 1995), vol. 19C, part IV, p.141.
[16] G. Saibene, M.L. Apicella, D.J. Campbell, et al., Controlled Fusion and Plasma Physics (Proc. 22nd Eur. Conf. Bournemouth, United Kingdom, 1995), vol. 19C, part II, p.121.
[17] A. Loarte, Proc. 12th PSI Conference, to be published in J. Nucl. Mat. (1996).
[18] Y. Shimomura, M. Keilhacker, K. Lackner, et al., Nucl. Fusion **23** (1983) 869.
[19] P.J. Harbour, A. Loarte, S. Clement, et al., J. Nucl. Mater. **196-198** (1992) 386.
[20] B. La Bombard, J. Goetz, C. Kurz, et al., Phys. Plasmas **2** (1995) 2242.
[21] L. Johnson and E. Hinnov, Jour. Quant. Spectrosc. Radiat. Transfer **13** (1973) 333
[22] A.V. Chankin, S. Clement, K. Erents, et al., Plasma Phys. & Control. Fusion **36** (1994) 1853.
[23] I. H. Hutchinson, B. La Bombard, J. Goetz, et al., Plasma Phys. Control. Fusion **37** (1995) 1389.
[24] B. LaBombard, J.A. Goetz, I Hutchinson et al., Proc. 12th PSI Conference, to be published in J. Nucl. Mat. (1996).
[25] G.D. Porter, S.L. Allen, M. Brown, et al., Phys. Plasmas **3** (1996) 1967. See also T. Petrie, et al., Proc. 12th PSI Conference, to be published in J. Nucl. Mat. (1996).
[26] R.D. Monk, D.J. Campbell, S. Clement, et al., Controlled Fusion and Plasma Physics (Proc. 22th Eur. Conf. Bournemouth, United Kingdom, 1995), vol. 19C, part III, p.293.
[27] R.D. Monk, A. Loarte, A.V. Chankin, et al., Proc. 12th PSI Conference, to be published in J. Nucl. Mat. (1996).
[28] L. Schmitz, B. Merriman, L. Blush, et al., Phys Plasmas **2** (1995) 3081.
[29] P.C. Stangeby, Nucl. Fusion **33** (1993) 1695.
[30] K. Borrass, P.C. Stangeby, Controlled Fusion and Plasma Physics (Proc. 20th Eur. Conf. Lisboa, Portugal, 1993), vol. 17C, part II, p.763.
[31] R.D. Monk, A. Loarte, A. Chankin, et al., Contrib. Plasma Phys. **36** (1996) 37.

[32] K. Guenther, A. Hermann, M. Laux, et al., J. Nucl. Mater. **176-177** (1990) 236.
[33] K. Guenther, Controlled Fusion and Plasma Physics (Proc. 22th Eur. Conf. Bournemouth, United Kingdom, 1995), vol. 19C, part I, p.433.
[34] S.J. Davies, P.D. Morgan, Y. Ul'Haq, et al., Proc. 12th PSI Conference, to be published in J. Nucl. Mat. (1996).
[35] H. P. Summers, ADAS Users Manual, JET Report JET-IR(94)06 (1994).
[36] D. Post, J. Nucl. Mater. **220-222** (1995) 143.
[37] T. Lovegrove, L.D. Horton, R.W.T. Koenig, et al, Controlled Fusion and Plasma Physics (Proc. 22th Eur. Conf. Bournemouth, United Kingdom, 1995), vol. 19C, part III, p.301.
[38] K. Sawada, T. Fujimoto, J. Appl. Phys. **78** (1995) 2913.
[39] D.A. Knoll, P.R. McHugh, S.Krasheninnikov, Phys. Plasmas **3** (1996) 293.
[40] K. Borrass, D. Coster, D. Reiter, et al., Proc. 12th PSI Conference, to be published in J. Nucl. Mat. (1996).
[41] K. Borrass, Nucl. Fusion **31** (1991) 1035.
[42] G.F. Matthews, S. Allen, N. Asakura, et al., Proc. 12th PSI Conference, to be published in J. Nucl. Mat. (1996).
[43] M. Laux, W. Junker, A. Hermann, et al., Controlled Fusion and Plasma Physics (Proc. 21th Eur. Conf. Montpellier, France, 1994), vol. 18B, part II, p.726.
[44] V. Mertens, W. Junker, M. Laux, et al., Plasma Phys. & Control. Fusion **36** (1994) 1307.
[45] H. Zohm, Plasma Phys. & Control. Fusion **38** (1996) 105.
[46] G. Vlases and the JET Team, Proc. 16th Int. Conf. Plasm. Phys. & Control. Fus. Res., Montreal (IAEA-CN-64/A4-1).
[47] M. Greenwald, J.L. Terry, S.M. Wolfe, et al., Nuclear Fusion **28** (1988) 2199.
[48] G. Saibene, D.J. Campbell, L.D. Horton, et al., Proc. 12th PSI Conference, to be published in J. Nucl. Mat. (1996).
[49] O. Gruber, A. Kallenbach, M. Kaufmann, et al., Phys. Rev. Let. **74** (1995) 4217.
[50] J. Lingertat, A. Tabasso, S. Ali-Arshad, et al., Proc. 12th PSI Conference, to be published in J. Nucl. Mat. (1996).
[51] H.Y. Guo, J.P. Coad, S.J. Davies, et al., Proc. 12th PSI Conference, to be published in J. Nucl. Mat. (1996).
[52] A. Taroni, G. Corrigan, R. Simonini, et al., J. Nucl. Mater. **220-222** (1995) 1086.
[53] A. Loarte, D.J. Campbell, S. Clement, et al., Controlled Fusion and Plasma Physics (Proc. 22th Eur. Conf. Bournemouth, United Kingdom, 1995), vol. 19C, part III, p.305.
[54] A. Taroni, G. Corrigan, L.D. Horton, et al., Controlled Fusion and Plasma Physics (Proc. 22th Eur. Conf. Bournemouth, United Kingdom, 1995), vol. 19C, part IV, p.297.
[55] G. Vlases and JET Team, Plasma Phys. & Control. Nucl. Fus. Res. (Proc. 14th Int. Conf. Plasm. Phys. & Control. Fus. Res.) vol.1 (1993) 287.

[56] A. V. Chankin, D.J. Campbell, S. Clement, et al., Plasm. Phys. and Control. Fusion **38** (1996) 1579.

[57] A. Loarte, Technical Meeting and Workshop on ITER Divertor Design, ITER. ITER-EDA Garching, Germany, February 1994.

[58] M. Laux, A. Hermann, R. Neu, et al., Controlled Fusion and Plasma Physics (Proc. 22nd Eur. Conf. Bournemouth, United Kingdom, 1995), vol. 19C, part III, p.97.

[59] D.J. Campbell and the JET Team, Proc. 12th PSI Conference, to be published in J. Nucl. Mat. (1996).

[60] C.F. Maggi, J.D. Elder, W. Fundamenski, et al., Proc. 12th PSI Conference, to be published in J. Nucl. Mat. (1996).

[61] H. Kastelewicz, R. Schneider and J. Neuhauser, Plasma Phys. Control. Fusion **37** (1995) 723.

[62] M. Keilhacker, K. Lackner, K. Behringer, et al., Physica Scripta **T2/2** (1982) 443.

[63] C.S. Pitcher, H.-S. Bosch, A. Carlson et al., Controlled Fusion and Plasma Physics (Proc. 22th Eur. Conf. Bournemouth, United Kingdom, 1995), vol. 19C, part III, p.245.

[64] R. Schneider, H.-S. Bosch, J. Neuhauser et al., Proc. 12th PSI Conference, to be published in J. Nucl. Mat. (1996).